Complement receptor *C3ar1* deficiency does not alter brain structure or functional connectivity across early life development

Hanna Lemmik[1], Eugene Kim[1], Eilidh MacNicol[1], Davide Maselli[2], Michel Bernanos[1], Zhuoni Li[3], Dauda Abdullahi[1], Esther Walters[1], Maria Elisa Serrano Navacerrada[1], Wuding Zhou[4], Aleksandar Ivetic[2], Diana Cash[1†*], Laura Westacott[5†*]

[1]Department of Neuroimaging, King's College London, UK [2]School of Cardiovascular and Metabolic Medicine & Sciences, King's College London, UK [3]Department of Forensic and Neurodevelopmental Sciences, King's College London, UK [4]Peter Gorer Department of Immunobiology, King's College London, UK [5]Neuroscience and Mental Health Innovation Institute, Cardiff University, UK

[†]These authors contributed equally

For correspondence: westacottlj@cardiff.ac.uk (LJW), diana.cash@kcl.ac.uk (DC)

Abstract

Previous studies suggest that genetic deletion of the complement C3a anaphylatoxin chemotactic receptor (*C3ar1*), a key component of the innate immune response, influences behaviours associated with psychiatric symptomatology in mice but when and where *C3ar1* is needed in the brain is not known. These questions are significant because, as a G-protein-coupled receptor (GPCR), human C3AR1 serves as a potential therapeutic target for disorders associated with complement dysregulation, such as schizophrenia. To provide a brain-wide assessment of developmental *C3ar1* activity, we used longitudinal tensor-based morphometry (TBM), fractional anisotropy (FA) from diffusion-weighted magnetic resonance imaging (dMRI) and blood oxygen-level dependent functional MRI (BOLD fMRI) in male and female *C3ar1*-deficient mice and wild-type littermates, with behavioural assessment in adulthood. Unexpectedly, we did not find robust *C3ar1*-dependent phenotype in any of these measures. Therefore, our study does not support neurodevelopmental hypotheses for *C3ar1* which will likely have implications for targeting this receptor in disease.

Introduction

The complement system is a conserved immune pathway that participates in host defence through pathogen clearance and regulating inflammation (Chaplin 2020) as well as tissue homeostasis (Kunz and Kemper 2021; West and Kemper 2023), with emerging roles in neurodevelopment, psychiatric disorders and neurodegeneration (Stevens et al. 2007; Hong et al. 2016; Sekar et al. 2016).

The most convincing evidence for the involvement of the complement system in neurodevelopment so far is its genetic association with schizophrenia. Schizophrenia is a complex and highly heritable neurodevelopmental disorder characterised by hallucinations, delusions, and impaired cognition, with symptoms typically emerging in late adolescence or early adulthood (McCutcheon, Reis Marques, and Howes 2020; Howes, Bukala, and Beck 2024). Neurobiological hallmarks of schizophrenia, among others, include grey matter loss (Vita et al. 2012) and a reduction in synaptic density (Osimo et al. 2019). Genome-wide association studies (GWAS) of schizophrenia have identified two complement-related risk loci, the complement component 4 A (*C4A*) structural variant (Sekar et al. 2016), which encodes C4A protein responsible for propagation of complement activation, and the CUB and Sushi Multiple Domains 1 (*CMSD1*) mutation which encodes a putative complement inhibitor protein (Schizophrenia Working Group of the Psychiatric Genomics Consortium 2014; Baum et al. 2024). Preclinical studies link these mutations to increased brain-specific complement activation and synapse loss (Sekar et al. 2016; Yilmaz et al. 2021; Baum et al. 2024) potentially tying complement activation to synaptic pathology in schizophrenia. Indeed, the *C4A* risk locus associates with MRI markers of grey matter loss and reduced cognitive performance in humans, even in the absence of neurological disorders (O'Connell et al. 2021). Complement pathway proteins represent promising therapeutic targets for disorders linked to abnormal complement activity. Complement modulation therefore has potential in addressing unmet therapeutic need in schizophrenia, since elevated complement proteins correlate with severity of negative symptoms in psychosis (Byrne et al. 2024), which do not respond to anti-psychotic medication.

C3a anaphylatoxin chemotactic receptor (C3aR1), a G-protein coupled receptor (GPCR) bound by complement activation product C3a and the granin family neuropeptide TLQP-21 (Rodriguez et al. 2023), acts downstream of complement activation and stands out as a pharmacologically tractable target for modifying complement activity in the brain (Hauser et al. 2017). In mice, its transcript is predominantly expressed by microglia, with minimal neuronal expression observed in both healthy adult humans and mice according to single-cell transcriptomic analyses (Hammond et al. 2019; Tasic et al. 2016). While its temporal expression patterns are not yet well characterised, it appears to be active during early embryonic development, potentially influencing progenitor cell proliferation (Coulthard et al. 2018; Bénard et al. 2008; Hammond et al. 2019). C3aR1 also appears to play a role in facilitating developmental astrocyte phagocytosis in the retina by microglia (Gnanaguru et al. 2023), as well as to regulate microglial reactivity and

neuroinflammation more broadly (Gedam et al. 2023; Ge, Guan, and Wang 2024; Zheng et al. 2021; Lian et al. 2015; Vasek et al. 2016; Chew and Petretto 2019). Brain morphological changes observed in *C3ar1*-deficient mice further support its neurodevelopmental relevance (Westacott et al. 2021; Pozo-Rodrigálvarez et al. 2021), although there is no consensus on the precise neurodevelopmental actions of C3aR1. Addressing this gap is important given its potential as a pharmacological target.

C3aR1 may impact brain functions relevant to psychiatric symptomatology since a range of behavioural phenotypes have been reported in *C3ar1*-deficienct mice. These include abnormal anxiety-like behaviours (Westacott et al. 2022), hyperactivity (Pozo-Rodrigálvarez et al. 2021), cognitive impairment (Coulthard et al. 2018) and resilience to depressive-like behaviours induced by chronic stress or inflammation (Crider et al. 2018; Zhang et al. 2022; Sun et al. 2024). The involvement of C3aR1 in behaviour suggests that it is needed for healthy brain function, but it remains unclear whether the observed phenotypes arise because C3aR1 is needed during development or from ongoing tonic activity, necessitating longitudinal assessment. Importantly, none of the aforementioned studies used control wildtype mice that were littermates of genetically *C3ar1*-deficient mice, which presents a confound due to the rapidly diverging genetic background between mutant and control in small inbred colonies (Fitch and Atchley 1985), but also because litter environment affects behaviour and brain development (Crews et al. 2009; Jiménez and Zylka 2021; Valiquette et al. 2023).

To investigate the potential effects of *C3ar1* deficiency, we adopted a global, unbiased approach, conducting a longitudinal study of male and female *C3ar1*-deficient mice and their wild-type littermates during adolescence and adulthood. Using structural and diffusion magnetic resonance imaging (MRI and dMRI), alongside resting state functional connectivity (FC) analysis of the blood oxygen level dependent (BOLD rsf) MRI signal, we aimed to assess whether the requirement for C3aR1 is implicated in brain structural development during adolescence—a critical period for psychiatric vulnerability (Westacott and Wilkinson 2022; Paus, Keshavan, and Giedd 2008)—or only becomes evident in adulthood.

Our imaging measures included tensor-based morphometry (TBM) which is a sensitive measure for mapping developmental impacts of genetic and immune perturbations (Nasseef et al. 2018; Ellegood et al. 2018; Guma et al. 2022; Kielar et al. 2012), white matter fractional anisotropy (FA) from dMRI to evaluate white matter organisation which is influenced by microglial activity in development (Chan et al.

2024; Falangola et al. 2023), and other connectivity metrics such as global efficiency and clustering coefficient to analyse brain network topology (Zhu et al. 2017; Forlim et al. 2024; Hadley et al. 2016). These techniques were complemented by behavioural testing in adult mice, measuring cognition and emotional reactivity through established paradigms like the open field (OF) test, elevated plus maze (EPM), novel object recognition (NOR), and prepulse inhibition (PPI), the three former paradigms being previously tested in *C3ar1*-deficient mice. Unexpectedly, we found no robust brain or behavioural phenotype in our datasets, challenging the previous interpretations for a neurodevelopmental role for C3aR1 under physiological conditions.

Results

Validation of the *C3ar1*^{tm1Cge} mutation

Although we used an established *C3ar1* knockout line, *C3ar1*^{tm1Cge} (Humbles et al. 2000), we performed our own validation of the mutation, for which we designed a 79-base pair (bp) amplicon targeting the putatively deleted region (**Figure 1**). PCR analysis of cDNA derived from bone marrow-derived macrophages–a cell type consistently reported to express *C3ar1* mRNA (Tao et al. 2021; Mommert et al. 2018; Mamane et al. 2009)–showed no detectable transcript in this region in the mutant animals (**Figure 1-i**), confirming the absence of the canonical transcript. We also investigated the possibility of an alternative transcript after an alternative start codon but found no transcript there either (**Figure 1-ii**, **Supplemental figure 1**). These results were further corroborated by quantitative PCR (qPCR, n = 8) in homozygous knockout animals in either M0-like or interleukin 4 (IL4)-induced M2-like macrophages (**Supplemental figures 2a-e**). Together, these results confirm that *C3ar1*^{tm1Cge} is a true loss-of-function or a "knockout" allele resulting in no *C3ar1* transcript.

C3ar1-deficiency does not influence total or regional brain volume

We conducted a longitudinal MRI study (referred to as cohort 1 hereafter or implied when cohort is not specified) to investigate potential genotype-related differences in brain structure and function using *C3ar1*^{tmCge} homozygous knockout mice (*C3ar1*$^{-/-}$, *C3ar1*-deficient) and their littermate wild-type control animals (*C3ar1*$^{+/+}$) (**Figure 2a**) on C57BL6J (Charles River, UK) background. Both groups underwent *in vivo* MRI in adolescence (postnatal day or PND27-31) and adulthood (PND81-92). Structural MR images were additionally collected *ex vivo* from the same mice sacrificed in adulthood after the *in vivo* scan to achieve higher isotropic

resolution (0.1 mm *ex vivo* vs 0.15 mm *in vivo*) and increased signal-to-noise ratio (SNR). We also conducted MRI in adulthood in an independent study cohort, which also represents a replication dataset, rereferred to as cohort 2.

We used tensor-based morphometry (TBM) analysis to estimate total brain volume and to map regional brain volume differences. There were no genotype dependent differences in total brain volume *in vivo* in adolescence (**Figure 2b**) nor in adulthood (**Figure 2c**) although in both groups female mice exhibited significantly smaller total brain volumes compared to males in adolescence. These sex differences were no longer observed in adulthood which aligns with previous findings (Guma et al. 2024).

Using TBM, no significant genotype-dependent differences in regional brain volume were detected in adolescence (**Figure 2d-i**). In adulthood (**Figure 2d-ii**), *C3ar1*$^{-/-}$ mice showed a significant ($p < 0.05$) volume increase in the right pretectal area, and subthreshold ($0.05 < p < 0.5$) increases in the left pretectal area and the right lateral thalamus *in vivo* but these differences were no longer observed in the same study cohort *ex vivo* despite improved spatial resolution (not shown), nor did we observe any genotype-dependent differences using TBM analysis in cohort 2 (not shown).

We did not observe any genotype-by-sex interaction effects in adolescence or in adulthood *in vivo*, or *ex vivo* in adulthood the same study cohort, nor cohort 2 (not shown).

While no reproducibly significant genotype effects in regional volume were observed in cohort 1, we detected sexually dimorphic effects (**Figure 2d-iii** and **2d-iv**). In adolescence, female mice had significantly larger volumes bilaterally in agranular insular cortex (AI), superior colliculus (SC), medial septum (MS) and in CA1 region of the hippocampus, whereas male mice had increased volumes in white matter areas including the olfactory tract, the corpus callosum, the hippocampal commissure, and notably also in the median preoptic nucleus (MEPO) which is well known to be larger in male rodents (Gorski et al. 1978) (**Figure 2d-iii, Supplemental figure 3** for absolute volume). Many of these sex differences were no longer observed in adulthood (see also **Supplemental figure 4** for cohort 2 data), but females showed larger relative volumes in the dorsal anterior cingulate cortex (ACAd), secondary motor cortex (MOs) and primary somatosensory cortex (SSp). Adult males had larger volumes in the medial preoptic area (MPO), medial amygdala (MEA) and the bed nucleus of stria terminalis (BST)–differences which are well documented sexual

dimorphisms (Hines, Allen, and Gorski 1992) and which were also observed *ex vivo* in this study cohort (**Supplemental figure 5**).

There were also no genotype differences in regional brain volumes over time from adolescence to adulthood, nor did we observe any sex-by-genotype interaction (not shown). Overall, female somatosensory and motor cortices increased more in volume between adolescence and adulthood than male (**Supplemental figure 6**), in line with the observed smaller differences in these areas in adulthood compared to adolescence.

To evaluate whether our study was sufficiently powered to detect genotype effects on regional brain volume, we analysed intra-group variability using a region-of-interest (ROI)-based approach. The coefficient of variation for grey matter ROI volume showed no differences between genotypes *in vivo* in adolescence (**Figure 2e**) and adulthood (**Figure 2f**), nor *ex vivo* in adulthood (**Figure 2g**). Variability was low, ranging from 4.2–5.5% *in vivo* and 4.2% *ex vivo*, while hippocampal variability remained below the neuroimaging gold standard of 5%, at 3.7–3.8% *in vivo* and 4.2% *ex vivo* (Lerch et al. 2012). These values suggest that our study was well-positioned to detect a genotype effect if one had been present.

***C3ar1*-deficiency does not influence fractional anisotropy**

To assess the potential impact of *C3ar1* deficiency on white matter integrity, we measured fractional anisotropy (FA) as an indirect marker of axonal microstructure (**Figure 3**). Using voxel-wise analysis, we observed sub-threshold ($0.05 < p < 0.5$) decreases in FA in *C3ar1*-deficient mice compared to wild-types (**Figure 3a**). In adolescence, these sub-threshold reductions were noted in the corpus callosum (CC) and optic tract (OPT, **Figure 3a**, upper panel), while in adulthood, they were primarily localised to the corpus callosum (**Figure 3a**, bottom panel). These sub-threshold differences were not observed in *ex vivo* scans. Female mice had sub-threshold decreases in FA *in vivo* at PND90 in the internal capsule and in the third ventricle (**Supplemental figure 7**) but this was again no longer observed *ex vivo*. We did not observe any sex-by-genotype interactions in our FA datasets (not shown).

In our ROI-based FA analysis, we focused on predefined white matter regions, hypothesising that FA alterations would primarily occur in areas containing axonal tracts due to increased microglial developmental phagocytosis in *C3ar1*-deficient mice (Gnanaguru et al. 2023; Falangola et al. 2023; Chan et al. 2024). In this analysis also, no significant genotype effects were observed in adolescence (**Figure 3b-i**) or adulthood (**Figure 3b-ii**). There were no genotype-dependent differences in the

extent of change but FA increased in all white matter areas except the olfactory tract between adulthood and adolescence (**Figure 3b-iii**), which is in line with the early maturation of the olfaction system in mice (Gretenkord et al. 2019).

***C3ar1*-deficiency does not influence global functional brain connectivity**

To evaluate global brain FC, which has been reported to be altered in other microglia gene knockouts (Filipello et al. 2018; Deivasigamani et al. 2023; Zhan et al. 2014), we estimated FC through analysis of BOLD signal time-courses with the assumption that the magnitude of correlation between these time-courses corresponds to the strength of FC. We calculated pairwise correlation coefficients between 36 (18 per hemisphere) grey matter regions. Non-zero correlation values were averaged across proportional progressively decreasing sparsity thresholds to preserve biologically meaningful weak correlations while minimising noise (Bassett et al. 2009). No genotype-dependent differences in global FC were observed in adolescence (**Figure 4a**), adulthood (**Figure 4d**) or in the change over time (**Figure 4g**).

We applied graph theory to characterise global brain network connectivity across all regions, focusing on two key metrics: clustering coefficient (**Figure 4b**, **e** and **h**) and global efficiency (**Figure 4c**, **f** and **i**), and applying the same strategy for proportional thresholding as for FC. The clustering coefficient reflects the tendency of nodes to form connected local clusters, with higher values indicating the presence of more highly interconnected subnetworks within the brain (Bullmore and Sporns 2009). Global efficiency refers to the average of shortest paths linking nodes in a network and can be a proxy of information integration abilities since it decreases with cognitive deficit (Berlot et al. 2016; Hawkins et al. 2020) and increases with development (Jiang et al. 2023). Clustering coefficient and global efficiency appeared higher in *C3ar1*-deficient animals at both time-points, but this was not significant (**Supplemental table 1)**. Further, we found no effects of genotype across global connectivity measures when we treated males and females as separate groups (**Table 1**, for *p* values, see **Supplemental table 2**).

FC, global efficiency and clustering coefficient appeared to increase with brain maturation when groups were combined, but this was only significant in the case of global efficiency when graph sparsity was lower, that is, when 30-50% of the strongest connections were retained, with small effect sizes observed (Cohen's d = 0.30-0.32). These findings indicate that while *C3ar1* deficiency did not result in alterations in global network properties under our experimental conditions, developmental changes in global efficiency were detectable.

C3ar1-deficiency has no detectable effect on functional brain networks

Since *C3ar1*-deficient mice did not show statistically significant changes in global connectivity metrics, we next examined specific networks after conducting *t*-tests for each FC pair between genotypes. For this we used two hypothesis-free approaches; false discovery rate (FDR) correction to identify strongly differing edges between genotypes, and network-based statistics (NBS) (Zalesky, Fornito, and Bullmore 2010) to detect network-level differences while controlling for family-wise error rate. Thresholding the resulting *t*-value matrices at $|t| \geq 2$ for adulthood and adolescence, and their changes over time (adulthood-adolescence; **Figure 5a**), no edges remained significant after FDR correction, indicating an absence of strongly differing functional connections between genotypes. Then, using NBS, which tests the likelihood of detecting a connected component of a specific size, we determined that the network sizes observed after thresholding at $|t| \geq 2$ (n = 68 at PND30, n = 15 at PND90, and n = 1 for change) could occur by chance in these datasets.

Given that neither the hypothesis-free approaches, the FDR correction and NBS, detected genotype-related differences, we focused on anxiety-related regions. This decision was motivated by prior evidence of anxiety-like behaviour in *C3ar1*-deficient animals (Westacott et al. 2022) and the inclusion of anxiety-specific tests in our behavioural battery. We calculated the mean absolute connectivity strength of 20 *a priori* selected anxiety-related regions. We did not detect an effect of genotype (**Figure 5b**), sex (**Table 2**) or a sex-by-genotype interaction (**Supplemental table 3**).

Next, we examined FC and global efficiency within resting state networks that have been linked to anxiety and emotionality in humans (Coutinho et al. 2016; Geng et al. 2015; Schimmelpfennig et al. 2023) and that have been observed in mice (J. Grandjean et al. 2020; Sforazzini et al. 2014; Hikishima et al. 2023), the default mode network (DMN) and the salience network (SAL; **Figure 5c**). Additionally, we analysed network connectivity within the predefined anxiety-related regions whose overall connectivity was summarised in **Figure 5b**. Consistent with our earlier findings, we did not observe genotype-dependent differences in these networks at either time-point.

The only significant genotype-related differences were seen in voxel-wise seed-to-brain connectivity analysis. Here, we show two anxiety-related regions, the left prefrontal cortex and left ventral hippocampus (**Figure 5d**; **Supplemental figure 8** for the right hemisphere) where we observed weak but significant, widespread higher connectivity in *C3ar1*-deficient animals compared to controls at both time-points.

Seed-based analysis further revealed higher FC across the brain when other anxiety-related regions were used as seeds, mostly in adolescence (**Supplemental figure 9**). However, this effect was not confined to anxiety-related regions or specific networks (**Supplemental figure 10**). Although the increase of FC in *C3ar1*-deficient mice appears widespread, this is not robust, since our seed-based analysis controls for voxel-wise comparisons within subjects but does not correct for testing multiple seeds.

***C3ar1*-deficient mice do not have any discernible behavioural phenotypes**

Another way of assessing functional consequences of genetic manipulations with expected neurodevelopmental sequelae is behavioural testing (Crawley 2007). In this study, we aimed to evaluate the impact of *C3ar1* deficiency on anxiety-like behaviour, locomotion and recognition memory, which were chosen based on prior reports of being altered in *C3ar1*-deficient mice. We used a battery of well-established behavioural tests, including the OF test and EPM for anxiety-like behaviour and locomotion, as well as NOR for recognition memory. We also tested PPI which is a sensorimotor reflex consistently found to be attenuated in schizophrenia (Ludewig, Geyer, and Vollenweider 2003; Mena et al. 2016) but has not been tested in *C3ar1*-deficient mice.

We performed behavioural testing in both cohorts described in the structural MRI results sections. In cohort 1 (**Figure 2a**), behavioural testing (EPM, then OF) occurred shortly before adulthood MRI scan. Behaviour of cohort 2 was also tested in adulthood (OF, NOR, EPM, PPI, in that order) followed by MRI, but they did not undergo an MRI scan in adolescence. Behavioural data were analysed separately for each cohort to account for differences in study design (see also Methods).

To assess anxiety-like behaviour and locomotion (**Figure 6a–b, Supplemental table 4** for description of anxiety-like metric selection), we calculated z-scores for *C3ar1*-deficient mice relative to wild-type controls (**Table 3** for untransformed means). In cohort 1, no significant genotype effects were detected on anxiety-like behaviour or locomotion at either time-point (**Supplemental table 5**). To address potential confounding from co-housing littermate mutants and wild-types (Kalbassi et al. 2017), we also examined whether the number of *C3ar1*-deficient cage-mates influenced wild-type behaviour (**Supplemental figure 11**) but found no consistent pattern or evidence of systematic anxiety-like effects in wild-types.

In cohort 2, most anxiety-related and locomotion measures showed no genotype differences (**Supplemental table 6**), except for reduced distance travelled in the

centre 70% of the OF arena by *C3ar1*-deficient mice (uncorrected two-sample *t*-test $p < 0.01$, Cohen's $d = 0.92$, **Supplemental table 6**). However, no genotype effect on distance was detected in the core 30% of the OF arena or in the centre and core of the OF arena in cohort 1.

The sample size (n = 38) of cohort 2 was insufficient to test sex-by-genotype interactions, limiting statistical power to detect only large effects (Cohen's $f = 0.5$ at alpha = 0.05 and 80% power), which were clearly not observed across behavioural measures. No sex-by-genotype interactions were observed in cohort 1 (**Supplemental table 5**).

Additionally, PPI testing in cohort 2 exclusively showed no effect of *C3ar1* deletion, though PPI increased with prepulse intensity as expected (**Figure 6c**). NOR testing (also exclusively in cohort 2) revealed no genotype differences, with all groups demonstrating successful learning based on recognition indices significantly above chance levels (**Figure 6d**).

Overall, these findings suggest that *C3ar1* deficiency does not result in robust anxiety-like or hyperactive phenotypes, nor deficits in recognition memory or PPI.

Discussion

Here we used a longitudinal neuroimaging and behavioural testing to investigate the impacts of *C3ar1* deletion on brain structure and function across early life development in mice. We found no robust evidence that *C3ar1* deficiency affects total or regional brain volume, white matter FA, global FC, global efficiency, clustering, or specific functional networks although we were able to detect previously reported sexual dimorphisms and brain maturation effects unrelated to *C3ar1* status in these datasets.

We also found no evidence of changed behavioural outcomes in male or female *C3ar1*-deficient mice in adulthood. These results raise questions regarding the source of discrepancies between these data, our previous behavioural work (Westacott et al. 2022; Westacott et al. 2021), and that of others (Crider et al. 2018; Coulthard et al. 2018; Pozo-Rodrigálvarez et al. 2021; Sun et al. 2024), which may be attributed to our use of littermate controls, as will be elaborated upon in the following sections. Overall, the lack of a behavioural phenotype combined with the paucity of genotype effects in brain structure across time-points suggest the role of C3aR1 in neurodevelopment and behaviour might not be as significant as originally thought, at least in the absence of exacerbating stress or immune triggers.

Absence of *C3ar1*-dependent effects on brain structure

Our morphometric analysis showed that total and regional brain volume was not changed between *C3ar1*-deficient and wild-type mice. We were, however, able to detect sex-specific neurodevelopmental changes that have previously been reported in rodents been such as brain growth occurring later in females and minimal total and regional brain volume differences in adulthood (Qiu et al. 2018; Guma et al. 2024; Gorski et al. 1978; Hines, Allen, and Gorski 1992; de Courten-Myers 1999), indicating that our method was sensitive enough to detect these. Given the low variability in our sample and our ability to detect these known sex differences, we believe our study was well-positioned to identify potential genotype effects, had they been present.

Absence of *C3ar1*-dependent effects on white matter fractional anisotropy

C3ar1 is predominantly expressed by microglia in the brain (Quell et al. 2017; Tasic et al. 2018), where it influences their reactivity and phagocytosis (Vasek et al. 2016; Gedam et al. 2023; Zheng et al. 2021; Lian et al. 2015; Gnanaguru et al. 2023), and developmental microglial characteristics are associated with FA changes in mice and humans (Falangola et al. 2023; Chan et al. 2024). In this study, we found no *C3ar1*-dependent changes in white matter while we were able to detect brain maturation effects on FA regardless of genotype, which increases during white matter development between adolescence and adulthood in both humans and mice (Brouwer et al. 2012; Hagmann et al. 2010; Reynolds et al. 2019; Piekarski et al. 2023; Chahboune et al. 2007). Lack of a phenotype after the deletion of a predominantly microglial gene may not be surprising in the light of recent report that suggest mice that have never had any microglia (achieved by deleting the super enhancer for macrophage colony-stimulating factor receptor, *Csf1r*) do not have overt neurodevelopmental phenotypes (Rojo et al. 2019), and only show severe vulnerability on a neuroinflammatory 5X-FAD background which is used to model Alzheimer's disease (Kiani Shabestari et al. 2022). It could therefore also be that *C3ar1*-deficient neurodevelopmental phenotypes can only be detected in the context of neuroinflammation.

Widespread, weak seed-to-brain functional connectivity increase in *C3ar1*-deficient mice in adolescence

We did not detect genotype-dependent global FC changes nor changes to clustering coefficient and global efficiency at either time-point, but we did observe a genotype-independent developmental increase in global efficiency with time which has been reported before (Jiang et al. 2023; Hagmann et al. 2010; Koenis et al. 2018),

particularly at lower sparsities (Cai, Dong, and Niu 2018), which similarly to out structural results indicates that our method was sensitive enough to pick up developmentally relevant effects.

Similarly, we did not observe any genotype-dependent changes to specific brain networks, including anxiety networks (**Figure 5**), which we previously hypothesised to be affected based on our previous behavioural results (Westacott et al. 2022). However, our anxiety network connectivity findings are internally consistent with the absence of an anxiety-like phenotype in the cohorts tested in this study. Combined with a recent null report for an anxiety-like effect in the EPM in *C3ar1*-deficient animals by another group (Sun et al. 2024), our data indicate that the effect of *C3ar1* on brain and behaviour correlates of anxiety-like behaviour must be context-dependent and/or minimal.

Although we did not detect network-specific effects, *C3ar1*-deficient mice exhibited widespread increases in resting-state FC in voxel-wise seed-based analyses during adolescence across nearly all seeds examined, with a weaker effect persisting into adulthood (**Figure 5** and **Supplemental figures 8-10**). These subtle increases in connectivity may reflect developmental alterations in circuit properties caused by the absence of C3aR1. For instance, similar findings have been reported for other microglial receptors—such as TREM2, CX3CR1, and CR3—where genetic deficiency altered adult brain FC (Filipello et al. 2018; Zhan et al. 2014; Deivasigamani et al. 2023). In these reports, TREM2 or CX3CR1 knockouts led to impaired synapse elimination alongside decreased FC, accompanied by social behaviour deficits and increased repetitive behaviour (Filipello et al. 2018; Zhan et al. 2014). In contrast, CR3 knockout mice exhibited no deficits in synapse or axon refinement but showed reduced phagocytosis of perinatal cortical neurons and higher cortical FC (Deivasigamani et al. 2023). It is indeed possible that similarly to CR3, C3aR1 is also involved in perinatal neuron phagocytosis so that its deletion results in weak brain-wide increase in FC, particularly as *C3ar1*-deficiency leads to a deficit of developmental astrocyte phagocytosis in the retina (Gnanaguru et al. 2023). For now, we urge caution with this interpretation for several reasons. First, these connectivity changes were not accompanied by any structural or microstructural alteration across the brain. Second, the voxel-wise seed-based analysis is the least robust presented here, as the observed changes were largely transient, weak, not confined to a specific subnetwork, and not corrected for multiple comparisons across seeds. Future studies investigating FC in *C3ar1*-deficient mice should incorporate repeat measures from the same individual during adolescence to improve robustness as well as measuring spontaneous and miniature excitatory synaptic current (sEPSC

and mEPSC respectively) in brain slices, although it is currently still unclear which brain regions should be targeted currently with the latter approach.

Behavioural outcomes were unaffected by *C3ar1* deficiency

Neither anxiety-like behaviours nor locomotor activity showed significant differences between genotypes across multiple testing paradigms, apart from a specific decrease in ambulation of *C3ar1*-deficient mice in the aversive central zone covering 70% of the open field, which in the absence of a locomotor phenotype could index anxiety-like processes. This latter change, however, was not reproducible across study cohorts and was no longer observed in the same study in the core of the open field, covering 30% of the arena. Tests for recognition memory and sensorimotor gating, NOR and PPI tests, also yielded null results.

Differences between our current findings and previous reports of anxiety-like behaviours (Westacott et al. 2022), hyperactivity (Pozo-Rodrigálvarez et al. 2021) and cognitive deficits (Coulthard et al. 2018) may stem from variations in experimental design, particularly environmental factors such as lighting and testing time. Our behavioural experiments were conducted during the active phase (7 PM–11 PM, lights off) to minimise stress from sleep deprivation, which is known to upregulate complement in the brain (Tillmon et al. 2024; Crider et al. 2018; Li et al. 2023; Tripathi et al. 2021). It is possible that previous studies, which tested animals during their inactive phase, introduced a stress-dependent "second hit" to *C3ar1*-deficiency. However, this seems unlikely since inhibiting complement, including *C3ar1*, has been shown to improve resilience to chronic stress (Li et al. 2023; Crider et al. 2018; Tripathi et al. 2021; Madeshiya et al. 2022; Tillmon et al. 2024).

Unlike previous studies of *C3ar1*-deficient mice, our study employed littermate control animals, meaning that wild-type mice were co-housed with their *C3ar1*-deficient siblings. This approach minimises potential environmental differences between groups, which is especially important in neurobehavioral studies where subtle environmental factors can significantly affect outcomes. While the use of littermate controls is widely regarded as best practice in such contexts (Holmdahl and Malissen 2012; Valiquette et al. 2023; Bailey, Rustay, and Crawley 2006), it is not without its own potential confounds. For instance, abnormal behaviours exhibited by genetically altered animals can influence the behaviour of co-housed wild-type mice, particularly when the phenotype is pronounced, such as in cases of increased aggression (Kalbassi et al. 2017). However, as aggression has not been reported in *C3ar1*-deficient mice, and their previously described behavioural phenotype was not notably severe, we considered such an influence unlikely in our study. Nevertheless,

461 we systematically examined whether the behaviour of wild-type mice correlated with
462 the number of *C3ar1*-deficient cage-mates and found no significant association
463 (**Supplemental figure 11**).

464 Prenatal environment and maternal care significantly influence phenotypic
465 development (McCarty 2017) and the complement system plays an essential role in
466 normal pregnancy and parturition (Girardi et al. 2020). A notable aspect of using a
467 littermate design is that litters of mixed genotype are born from exclusively
468 heterozygous parents, whereas in most prior studies of *C3ar1*-deficiency both the
469 mother and offspring were homozygous knockouts. This raises the possibility that
470 behavioural effects in *C3ar1*-deficient mice may result from altered intrauterine
471 environments or maternal care by *C3ar1*-deficient mothers. In line with this, our
472 inbred homozygous *C3ar1* knockout colony showed increased pre-weaning deaths
473 and maternal cannibalism (unpublished data). If this is indeed the reason for
474 previously observed adult behavioural phenotypes, two scenarios should be
475 considered. In the first scenario, the adult phenotypes are specific and *C3ar1-*
476 deficient offspring are uniquely sensitive to C3aR1-dependent *in utero* conditions or
477 maternal care deficits. In the second, more likely scenario, however, the adult
478 phenotypes are not specific to *C3ar1*-deficiency (i.e., wild-type mice would have
479 been similarly affected). If the latter is true, we were able to avoid measuring these
480 non-specific effects by using a littermate design.

481 Null results in our global knockout model could also be due to genetic
482 compensation, where genes with similar function compensate for the loss of a
483 mutated gene (El-Brolosy and Stainier 2017). While the mechanism for this is not yet
484 resolved, mutated RNA degradation can trigger this process (El-Brolosy et al. 2019).
485 We confirmed that the *C3ar1*^{tm1Cge} mutant lacks detectable *C3ar1* RNA, suggesting
486 the transcript is either not produced or undergoes nonsense-mediated decay,
487 potentially activating compensation. Confirming this would require longitudinal
488 single-cell RNA sequencing in relevant brain regions, which is beyond the scope of
489 this study.

490 Genetic background of transgenic models is another factor that varies between
491 laboratories and is known to affect phenotypic expression. For example,
492 heterozygous knockout of the autism-associated gene *CHD8* has varying effects in 33
493 (Tabbaa, Knoll, and Levitt 2023) substrains, mirroring heterogeneity observed in
494 human *CHD8*-haploinsufficiency. While that study identified significant variability
495 across substrains, these profiles consistently differed from that of wild-type littermate
496 controls. In contrast, our study found no robust genotype-dependent differences in

the brain globally and across measures or in behaviour, apart from a single internally non-reproducible behavioural outcome measure, meaning that the effect of C3aR1 on brain development would have to be entirely dependent on modifying genes or environmental factors.

Finally, genetic drift could have precluded reproducibility of previously reported phenotypes. Mice accumulate spontaneous mutations that rapidly reach homozygosity within small colonies speeding up drift, a phenomenon recognised as early as the 1980s (Fitch and Atchley 1985). So far, our current work is the first to study *C3ar1* deficiency using a littermate design, which minimises the number of genetic loci that differ between the mutant and control mice, all of which could influence measured phenotypes. Fully understanding the genetic causes of results previously observed by our laboratory and others would require systematic outcrossing, whole genome sequencing, and linkage analysis. Given that hundreds of genes likely differ between mutant and control lines last crossed during mutation creation or before, the value of such work is questionable.

Future directions

Aside from the role of C3aR1 in brain structure and function, many aspects of the basic biology of C3aR1 remain unclear, including its expression pattern in the healthy brain, with little information available on the cell types, contexts, or time-points where it is expressed. It is also unclear which G-proteins C3aR1 signals through in different brain cell types. Future studies could integrate toolkits like TRUPATH, a suite of Gαβγ biosensors for analysing G-protein coupling preferences (Olsen et al. 2020), with transcriptomics to address these questions. This approach would be particularly valuable, as it could enable the use of chemogenetics to activate the same G-protein as C3aR1 in specific cell types and contexts to study its function.

Most importantly, we propose that *C3ar1*-deficiency in development should be studied after an immune challenge. Unlike humans, laboratory mice live in an immune-privileged environment, hence investigating the consequences of a combined immune insult with the genetic deficit would be relevant; or better yet, in the context of *C4A* overexpression, which is a known genetic risk factor for schizophrenia (Sekar et al. 2016) and is known to impact white matter integrity (Caseras et al. 2024).

530 **Limitations**

531 In this study, we provided high-level global data on *C3ar1*-deficient mice. While our
532 study had notable strengths, including the use of a littermate design and the
533 inclusion of female animals, it is not an exhaustive characterisation of the mutant.

534 While we measured brain region volumes, we cannot definitively address more
535 reductionist questions, such as cellular composition which would have required
536 antibody staining and microscopy. Similarly, for axonal integrity analysis for which
537 we used the proxy of dMRI-derived FA, the gold standard would have been electron
538 microscopy. However, a more granular approach would have necessitated a trade-off
539 with throughput–something that is hard to justify in the absence of strong
540 hypotheses regarding the developmental expression pattern of *C3ar1*. Additionally,
541 our neuroimaging functional analysis relied on a specific parcellation of the brain
542 consisting of 36 regions, and different parcellations could yield varying results
543 (Thirion et al. 2014; Zalesky et al. 2010). We encourage others exploring our datasets
544 to therefore experiment with alternative parcellations.

545 **Conclusion**

546 Contrary to expectations, we found no evidence for *C3ar1*-dependent effects across
547 imaging measures at either time-point nor could we replicate previously seen
548 behavioural phenotypes. The absence of detectable phenotypes suggests that C3aR1
549 plays a minimal role in brain development, at least in the absence of an immune
550 trigger. These findings challenge prior assumptions about its neurodevelopmental
551 significance and necessitate further investigation into C3aR1 function on sensitized
552 backgrounds, such as those involving immune activation.

553 Methods and materials

554 **Animals**

555 All animal procedures complied with the UK Animals and Scientific Procedures Act
556 1986 and were approved by the local ethical committee at King's College London
557 (KCL). Homozygous *C3ar1*$^{-/-}$ mice were generated by homologous recombination in
558 embryonic stem cells and kindly provided by Dr. Bao Lu and Prof. Craig Gerard
559 (Harvard Medical School, Boston, MA) (Humbles et al. 2000). These mice were
560 subsequently backcrossed onto the C57BL/6J strain for at least 12 generations and
561 maintained on a C57BL/6J background in Professor Wuding Zhou's laboratory at
562 KCL. For this study, cryopreserved stocks were rederived at KCL and crossed to

563 C57BL/6J mice purchased from Charles River to refresh the genetic background
564 following Jackson's Laboratories line refreshing protocol.

565 Experimental animals (*C3ar1*$^{-/-}$ and *C3ar1*$^{+/+}$ littermates) were generated through
566 heterozygote incrosses and resulting genotypes followed Mendelian ratios. The
567 heterozygote breeders were generated by outcrossing heterozygous mice to bought
568 wild-type Charles River C57BL/6Js. The breeders used to produce the experimental
569 animals were derived either from the first, second or third of these outcrosses. Sibling
570 crosses were not conducted and parental age was between 2-4 months to minimise
571 genetic drift.

572 Experimental mice were housed in individually ventilated cages under controlled
573 temperature (20–25°C), humidity (50–60%), and a 12-hour light-dark cycle (lights
574 on at 7:00 AM, lights off at 7:00 PM). Environmental enrichment included nesting
575 materials, tunnels, and chew sticks. Mice had *ad libitum* access to irradiated rodent
576 chow and autoclaved water. Animals were group-housed (2–4 mice per cage), with
577 males and females housed separately after weaning (PND21±2). Genotyping was
578 conducted on ear biopsy DNA by Transnetyx using probes targeting the neomycin
579 cassette for the mutant allele and intron 1 for the wild-type allele. No mismatches
580 were identified through double-genotyping 20% of the study cohorts.

581 **Validation of mutation**

582 Bone marrow-derived macrophages were obtained from tibias and femurs of eight
583 three-month-old mice (n = 4 *C3ar1*$^{+/+}$, n = 4 *C3ar1*$^{-/-}$) following standard protocols.
584 Bone marrow was filtered through a 40 μm mesh, centrifuged at 450 x g for 5
585 minutes at 4°C, and treated with NH4CL haemolysis buffer (NH4CL 0.15M,
586 K2HCO3 0.01M, EDTA 0.0001M). After a second centrifugation under the same
587 conditions, cells were washed with PBS and resuspended in Gibco RPMI 1640
588 Medium (Thermo Fisher, #21875-034) supplemented with 50 ng/ml recombinant
589 mouse macrophage colony-stimulating factor (M-CSF, R&D Systems, #416-ML-
590 010/CF), 1% penicillin, 1% streptomycin, and 10% heat-inactivated fetal bovine
591 serum (Sigma, #F9665-50ml).

592 Cells were seeded at 1x10^{6} cells/ml in six-well plates (six wells per animal) and
593 incubated at 37°C with 5% CO_2 for 72 hours. On day three, fresh medium was
594 replaced, and 50 ng/ml recombinant mouse IL4 (R&D Systems, #404-ML-
595 010/CF) was added to half of the wells to skew them towards M2 phenotype.
596 Incubation continued for an additional 48-72 hours, depending on cell confluence.

597 RNA was extracted using the ReliaPrep™ miRNA Cell and Tissue Miniprep
598 System (Promega, #Z6211) according to the manufacturer's instructions. RNA
599 concentration was determined with a NanoDrop spectrophotometer (Thermo
600 Scientific, NanoDrop 2000), yielding values between 25.5 ng/µl and 227.5 ng/µl.
601 Reverse transcription PCR (RT-PCR) was performed using the LunaScript® RT
602 SuperMix Kit (NEB, #E3010L), again following the manufacturer's instructions.
603 Depending on RNA yield, either 100 or 500 ng of RNA was used per reaction.

604 For cDNA PCR and gel electrophoresis, we used GoTaq® G2 Master Mix (NEB,
605 #M7822). We amplified a 79 basepair (bp) fragment in the deleted region alongside a
606 372 bp region in the *C3ar1* cDNA that was located outside the deleted region and
607 downstream of an alternative start codon identified through Benchling. *Gapdh*
608 primers were included in each reaction to confirm amplification efficiency. PCR
609 products were analysed on a 2% agarose gel stained with GelRed.

610 For qPCR, we amplified the previously mentioned 79 basepair (bp) fragment in the
611 deleted region. Samples were analysed in triplicate on 96-well plates (Applied
612 Biosystems, #4346906) with Luna® Universal qPCR Master Mix (NEB, #M3003L)
613 and readings were obtained using an Applied Biosystems StepOnePlus plate reader.
614 The amplification data were processed with the $^{\Delta\Delta}$Ct method, normalising against
615 the housekeeping gene, Hypoxanthine phosphoribosyltransferase 1 (*Hprt*).
616 Genotypes were arranged alternately across the plate to minimise bias. To verify M2-
617 like polarisation, the expression of M2-specific markers Arginase 1 (*Arg1*) and the
618 mannose receptor, Cluster of differentiation 206 (*Cd206*) were assessed.

619 **Table 4 | Primer sequences**

Primer name	Forward	Reverse	Application
C3ar1	AGGATTTGTTGGTG GCTCGCA	CTCCATGGCTCAGTC AAGCACA	PCR and qPCR deleted region
C3ar1	GCTTCCTGGTGCCG TTTTTC	AGTTGGTAGAGTGCG TGAGC	PCR of putative alternative transcript (3' end of exon 2 after alternative start codon)
Hprt	AGTCCCAGCGTCGT GATTAGCG	TTGAGCACACAGAGG GCCACAA	qPCR housekeeping gene
Arg1	GGCTTGCGAGACGT AGACCC	GTCCAGCCCGTCGAC ATCAAA	qPCR verification of M2 polarisation
Cd206	CCGGAGGGTGCAGA CAAAGG	TCGTCCACAGTCCAC CGAAAC	qPCR verification of M2 polarisation

Gapdh	CCTAGACAAAATGG TGAA	GACTCCACGACATAC TCAGC	PCR amplification efficiency control

Table 5 | PCR reaction

Amount (µl)	Reagent
12.5	GoTaq® G2 Master Mix (Green)
1	*C3ar1* forward primer, 10 mM
1	*C3ar1* reverse primer, 10 mM
1	*Gapdh* forward primer, 10 mM
1	*Gapdh* reverse primer, 10 mM
7.5	H_2O
1	Template DNA
Final volume: 25 µl	

Table 6 | Cycling conditions

Step	Time	Temperature
1. Initial denaturation	5 min	94°C
2. Denaturation	30 sec	94°C
3. Annealing	30 sec	60°C
4. Extension	1 min	72°C
5. Repeat steps 2-4	Repeat 35 x	
6. Final extension	5 min	72°C

Study design

This study used two separate cohorts of male and female *C3ar1*-deficient and littermate wild-type mice. The main, longitudinal MRI cohort termed cohort 1, had *in vivo* MRI performed in adolescence (range 27-31 days) and adulthood (range 81-92 days), and the adulthood MRI scan was preceded by OF and EPM tests. The adolescence time-point was chosen because mice reach puberty approximately between PND24-34 (Semaan and Kauffman 2015; Brust, Schindler, and Lewejohann 2015; Pintér et al. 2007). *Ex vivo* imaging was conducted in cohort 2's perfusion-fixed brains after the final adulthood scan.

For cohort 2, behavioural testing was conducted similarly to cohort 1 in adulthood only (range 74-110), and consisted of OF, NOR, EPM and PPI followed by *in vivo* structural and diffusion MRI (note that MRI was not conducted in adolescence in this cohort). For both cohorts, behavioural testing was conducted 2-7 days before the adulthood scan.

638 Sample size of cohort 1 was statistically powered to detect medium effect sizes in
639 regional volume using TBM across four groups (males and females analysed
640 separately), with a minimum sample size of n = 15 per group based on previously
641 observed variance with this method by our group (Serrano et al. 2023). For cohort 2 ,
642 statistical power was calculated to detect medium effect sizes in regional TBM with
643 sexes combined, using a sample size of n = 16 per group.

644 ***In vivo* MRI**

645 Two to three days after behavioural testing, mice were imaged using a Bruker
646 BioSpec 9.4 T scanner with an 86-mm volume resonator for transmission and a 4-
647 channel surface array coil. Anaesthesia was induced with 4% isoflurane in medical air
648 (1 L/min) and oxygen (0.4 L/min), maintained at 2% but adjusted based on
649 respiration rates. For functional BOLD MRI in cohort 1, we used a medetomidine
650 and isoflurane anaesthesia optimised for mouse fMRI (Joanes Grandjean et al. 2014).
651 This consisted of a subcutaneous medetomidine bolus (0.05 mg/kg) followed ten
652 minutes later by its continuous infusion (0.1 mg/kg/h), with isoflurane levels
653 gradually reduced to 0.45-0.65% over 15 minutes from the start of the infusion after
654 BOLD-weighted fMRI was conducted after the structural scans which took a further
655 45-60 minutes after reducing isoflurane level. The respiration rate was monitored
656 with a pressure sensor, and temperature was monitored with a rectal thermometer
657 and maintained at 36-37°C using a water circulation system.

658 ***Ex vivo* MRI**

659 Following the adulthood *in vivo* scan in cohort 1, mice were perfused transcardially
660 with 20 mL phosphate-buffered saline (PBS) followed by 4% paraformaldehyde
661 (PFA). Heads were stored in PFA for 48 hours, then transferred to PBS containing
662 0.05% sodium azide and 2 mM gadolinium-based contrast agent (Gd-DO3A-butrol).
663 Brains were scanned *in cranio* in groups of four using a custom-made holder
664 immersed in perfluoropolyether (Galden®, Solvay).

665 **MRI acquisition parameters**

666 For *in vivo* imaging, we first acquired an Actual Flip Angle Imaging (AFI) sequence
667 for B1 mapping. Then we acquired three types of 3D multi-gradient-echo images
668 that were used for creating study-specific templates: magnetization-transfer weighted
669 (MTw), proton-density weighted (PDw), and T1-weighted (T1w). Subsequently,
670 T2-weighted Rapid Acquisition with Relaxation Enhancement (RARE) images were
671 obtained. Diffusion-weighted images were then acquired using a single-shot spin-
672 echo echo planar imaging (EPI) sequence. Finally, for the longitudinal MRI study,

BOLD rsfMRI data were acquired using a single-shot gradient-echo EPI sequence with 720 repetitions. Additionally, spin-echo EPI image pairs with opposing phase-encoding polarity were recorded to enable correction of susceptibility-induced distortions. The *in vivo* scanning session lasted 1-1.5 hours.

For *ex vivo* morphometric analysis, 3D T2-weighted images were acquired using RARE sequences, with a total scan duration of 1 hour and 5 minutes. Ex vivo diffusion-weighted images were obtained using Stejskal-Tanner pulsed gradient spin-echo sequences with a 3D segmented EPI readout. Three b0 images were collected at the beginning of three blocks of 30 diffusion-weighted images. The total scan time for this acquisition was 14 hours and 15 minutes.

Table 7 | MRI acquisition parameters

Image type	TR (ms)	TE (ms)	Flip angle (°)	Aver-ages	Band-width (kHz)	FOV	Matrix	Other
AFI	20/ 100	2.85	55	1	25	16.2 x 16.2 x 9	42 x 42 x 24	
MTw	24	2.5	6	2	100	16.2 x 16.2 x 9	108 × 108 × 60	6 echoes with 2.1 ms spacing; MT pulse: gaussian, 4 ms, amplitude 10 μT, offset -3 kHz, bandwidth 685 Hz
PDw	20	2.5	4	2	100	16.2 x 16.2 x 9	108 × 108 × 60	7 echoes with 2.1 ms spacing
T1w	20	2.5	20	2	100	16.2 x 16.2 x 9	108 × 108 × 60	7 echoes with 2.1 ms spacing
T2w in vivo	5000	42	90/ 180	4	50	16 x 12	128 × 96	32 slices, slice thickness 0.5, RARE factor 8
T2w ex vivo	300	30	90/ 180	1	50	25 x 24 x 18	250 x 240 x 180	RARE factor 4, scan time = 1 h 5 min

DWI in vivo	3000	21	90/ 180	2	357	19.2 x12	96 x 60	Single shot spin-echo planar imaging, 30 slices, slice thickness 0.5 mm, three diffusion shells: b = 350 s/mm^2 with 9 directions, b = 1000 s/mm^2 with 34 directions, b = 2000 s/mm^2 with 78 directions (δ = 3 ms, Δ = 11 ms), 3 b0 images per shell
DWI ex vivo	300	28.5	90/ 180		300	25 × 24 × 18	200 × 192 × 144	Stejskal-Tanner pulsed gradient spin echo sequences with a 3D segmented EPI readout. 12 segments and a total of 90 diffusion-weighted images acquired at a b-value of 4000 s/mm^2 (δ = 4 ms, Δ = 13 ms)
BOLD fMRI	1000	15	55	1	200	20 x 20	64 x 64	Single-shot gradient-echo EPI sequence, 16 slices, slice thickness 0.5, 720 repetitions

Structural MR image processing

For preprocessing MTw, T1w, and PDw images, de-ringing was conducted using the MRtrix3's (Tournier et al. 2019) `mrdegibbs` command. MTw, T1w, and PDw images were averaged across echo times, rigidly co-registered using Advanced Normalization Tools (ANTS; Avants et al. 2011) `antsRegistration`, and used for template construction (see below).

For DWI, MRtrix3 `dwidenoise` was used for de-noising, MRtrix3 `mrdegibbs` for de-ringing, and FSL's (the FMRIB Software Library, Jenkinson et al. 2012; Smith et al. 2004) `topup` and `eddy` for susceptibility and eddy-current distortion and motion correction. FSL's `dtifit` was used for diffusion tensor imaging (DTI) model fitting,

enabling the calculation of fractional anisotropy (FA), mean diffusivity (MD) and axial diffusivity (AD), the latter two which are not reported in this manuscript for brevity. For a more detailed diffusion processing protocol see Kim et al. (2023).

Study templates

The `antsMultivariateTemplateConstruction2.sh` script from ANTs was used to create study specific templates from processed images. For *in vivo* scans of cohort 1, MTw, T1w, R2* map (generated from the multi-gradient-echo PDw, T1w and MTw images using the `qi mpm_r2s` command in the QUIT package), S0, FA and MD images were used. For the *ex vivo* scans of cohort 1, separate T2w and DTI (comprising S0, FA, and MD images) templates were created. For cohort 2, PDw, T1w, MTw, S0 (estimated non-diffusion-weighted image from `dtifit`), FA, and MD images were used.

Jacobian determinant maps

To estimate volume, Jacobian determinant maps were generated from the deformation fields corresponding to the transformation of each subject to the study template using the `CreateJacobianDeterminantImage` command from ANTs. The Jacobian determinant values of all voxels within the template brain mask were summed to obtain the total brain volume of each subject. Jacobian determinants were calculated from the combined rigid, affine, and Symmetric Normalization (SyN) transforms as well as from only the SyN transforms to obtain maps of absolute and relative volume (accounting for differences in global brain volume), respectively. For TBM, the Jacobian determinants were subsequently log-transformed.

Voxel-wise analysis

For voxel-wise statistics, FSL randomise with permutation testing was used (10,000 for cohort 1, 5000 iterations for cohort 2) followed by a threshold-free cluster enhancement (TFCE) and family-wise error (FWE) correction as described in Wood et al. (2016) and Kim et al. (2023). Given the absence of genotype differences in total brain volume, TBM regional volumes are reported relative to total brain size for greater accuracy (Lerch et al. 2012), while absolute volume maps are reported in the Supplementary files where sex differences in total brain volume were present.

Common coordinate space

The study template was registered to the Allen Mouse Brain Common Coordinate Framework (CCFv3; Wang et al. 2020) using ANTs, and the Allen atlas was subsequently transformed to the study template space with the inverse transform.

ROI-based analysis of volume

The images were segmented using an in house modified version of the Allen atlas of 72 regions (Serrano et al. 2023; Wang et al. 2020). These segmentations were subsequently used to compute regional volumes by summing the Jacobian determinants within each parcellation.

Regional volume variability was estimated by calculating a coefficient of variation (CV) for each region with normalised root-mean-square method for each genotype in each experiment, using the calculation: $CV = \frac{\sigma}{\mu}$, where σ is the standard deviation and μ the population mean for each region in the atlas (n = 72 regions). Group differences in CV were calculated with a Kruskal-Wallis test (SciPy.stats, `kruskal`).

Fractional anisotropy

For mass-univariate voxel-wise analysis of fractional anisotropy, values from `dtifit` for cohort 1 were again analysed with FSL randomise with permutation testing (10,000 permutations) followed by TFCE and FWE-correction. FA is not reported for cohort 2 in this manuscript for brevity. For ROI-based analysis, voxel FA medians within parcellation were used for all white matter regions.

To calculate the change over time in fractional anisotropy in the longitudinal study, adolescence values for each voxel value or regional median were subtracted from adulthood values. Differences between genotypes were calculated with a mixed ANOVA with between-subjects factor of genotype and within-subjects factor of region. Change from 0 was calculated with a two-sided one-sample *t*-test (SciPy.stats, `ttest_1samp`), which was corrected with the Benjamini–Hochberg method.

BOLD fMRI pre-processing

Images were largely pre-processed using the Analysis of Functional NeuroImages (AFNI) toolkit. Slice timing correction was performed using the `3dTshift` package, despiking with `3dDespike`, and motion correction was applied with `3dvolreg`. The motion-corrected time average was then registered to each subject's own T2w image using ANTs, followed by registration to a template T2w image derived from a separate mouse study conducted at the BRAIN Centre (KCL). The use of this external template was justified by the low resolution of fMRI, which does not benefit from creating a study-specific template.

The images were also distortion corrected using FSL's `topup`, with the distortion estimated using auxiliary phase encoded spin-echo images with otherwise matching

acquisition parameters to the gradient echo EPI used for the BOLD signal. Prior to analysis, corrected images were band-pass filtered at 0.01–0.2 Hz with AFNI's `3dTproject` to remove low-frequency scanner drift noise and high-frequency physiological noise. Nuisance variables (movement and CSF signal) were also simultaneously regressed out of the signal at this stage. Finally, spatial smoothing was applied using AFNI's `3dBlurInMask` with a FWHM kernel.

Functional connectivity and graph theory analysis

For functional analysis, a high-level parcellation scheme was applied to segment 36 regions (18+18) excluding white matter from the acquired 3D volume. The BOLD signal time-courses were averaged within each ROI, and the mean time-courses were extracted using FSL's `fslmeants` tool. Pearson correlation coefficients were calculated for each time-course pair, producing a 36×36 correlation matrix for each subject. These matrices were analysed as functional connectivity (FC) graphs, with edge strength determined by the Fisher z transformed Pearson correlation coefficient. To identify the strongest connections, graphs were thresholded at 5% intervals from 5% to 50%. At each threshold level, referred to as the graph sparsity interval, connections below this threshold were set to zero, generating 10 sparsity graphs per subject. FC was calculated as the average non-zero connectivity at each threshold level. Global graph metrics, global efficiency and clustering coefficient, were computed at each sparsity level using Brain Connectivity Toolbox algorithms (Rubinov and Sporns 2010) implemented with Network X (3.4.2) `global_efficiency` and `clustering` passing binary thresholded Pearson matrices to prioritise topology in the presence of noise. For global efficiency and clustering coefficient, random curves were calculated by shuffling the thresholded binary matrix positions. Area under the curve (AUC) was computed per subject using trapezoidal numerical integration (`numpy.trapz`), and the likelihood of observed values was estimated with permutation testing (10,000 permutations).

To estimate changes over time, global graph metric values at adolescence were subtracted from adulthood values at each sparsity interval. Group differences were again tested by calculating the AUC and applying permutation testing. Changes from baseline (zero) were evaluated using two-sided one-sample *t*-tests (difference from 0), corrected for multiple comparisons with the Benjamini-Hochberg method.

FDR correction and network-based statistics

Matrices for *C3ar1*-deficient and wild-type mice were compared with Student's *t*-tests for each pairwise connection, resulting in 36×36 *t*-statistic and *p*-value matrices.

To control for multiple comparisons, FDR correction was applied to the upper triangle of the *p*-value matrix using the Benjamini-Hochberg procedure (`statsmodels.stats.multitest.fdrcorrection`, $\alpha = 0.05$).

For network based statistics (NBS), above described *t* matrices were thresholded at $|t| \geq 2$. To identify connected components within the FC graph, adjacency matrices representing significant connections ($|t| \geq 2$) were converted into graph objects using NetworkX. Regions of interest (ROIs) were treated as nodes, and significant connections as edges. Connected components were identified using a breadth-first search (BFS) algorithm, which explores all neighbouring nodes before moving deeper into the graph. Only components containing more than one ROI were retained for further analysis. To generate a null distribution of maximal component sizes, group labels were randomly shuffled across subjects for each permutation while preserving matrix structure (10,000 permutation). The *p*-value for an observed component was calculated as the proportion of permutations where the maximal component size exceeded that of the observed component.

A priori **node strength analysis**

We selected 20 (10+10 left and right) anxiety and fear related regions and calculated their average absolute connectivity to all other regions using Fisher z-transformed Pearson correlation coefficients. We then used a mixed ANOVA with between-subjects factor of genotype and within-subjects factor of region followed by pairwise testing with BH FDR correction of *p* values.

Within-network analysis

Two mouse resting state networks were subset from correlation matrices: the default mode network (DMN) and the salience network (J. Grandjean et al. 2020; Sforazzini et al. 2014). The DMN included bilateral prefrontal cortices, cingulate cortices, and dorsal hippocampi, while the salience network comprised bilateral cingulate cortex, amygdala, and striatum. Additionally, a third anxiety-related network was defined, consisting of regions identified in the seed-based analysis described above.

For each network, mean FC was calculated as the average of all pairwise connections between nodes within the network, without applying a threshold. For individual network global efficiency analysis, thresholding was not used due to small amount of nodes. Instead, weighted Pearson matrices were passed to bctpy (0.6.1) `efficiency_wei`.

Student's *t* tests were used to test significance, and the comparisons were corrected within outcome measure with BH method.

Voxel-wise seed-to-brain analysis

We conducted voxel-wise seed-based FC analyses for anxiety-related regions, as well as the colliculus and sensory cortex, which served as control regions not specific to anxiety. For each seed region, the time-course of the BOLD signal was extracted and regressed with the BOLD signal of every voxel in the brain, resulting in a 3D spatial map of the connectivity with the seed. Group-level comparisons of these maps were performed between genotypes using voxel-wise permutation tests with FSL's randomise (5000 permutation), converted with TFCE and statistical significance corrected for multiple comparisons using FWE (seed-to-brain), but they were not corrected for the presence of multiple seeds.

General behavioural procedures

For cohort 1, EPM was administered as the first test, followed by OF. For cohort 2, OF was the first test, followed by NOR test after two days of low light habituation (4 lux), EPM, and PPI.

Handling of the mice began 2-3 days prior to the behavioural testing battery. By the start of the experiments, the mice sat comfortably on the experimenter's hand. Mice were handled using cardboard tunnels to minimise stress, and tail handling was avoided.

Behavioural tests were conducted during the dark phase (between 7:00 PM and 11:00 PM clock-time) of the light-dark cycle to align with the active period of mice. Mice were randomised by genotype and counter-balanced by sex, with the experimenter systematically blinded to genotype throughout testing and analysis though the allocation of a study ID and test order ID respectively.

For cleaning of the test apparatus, we used 70% EtOH for all arenas except for the EPM arena for which we used Virusolve (Amity International) to avoid damage to the material. Behaviour was recorded using a Google Pixel 5a camera at 1080p/60 fps. Videos were then cropped and down sampled by shell scripting using FFmpeg.

Open field test

Mice were placed in a 40 x 40 x 40 cm white arena and allowed to explore freely. For cohort 1, dim red light (4 lux) was used, while for cohort 2, the OF test was conducted under bright overhead lighting (500 lux). 10-minute videos were analysed

using CleverSys (VA, USA). Outcome parameters included time spent in the centre, total distance travelled, velocity, and thigmotaxis (edge exploration).

Novel object recognition

Cohort 2 mice were initially habituated to the arena under low light conditions (4 lux) over two days, five minutes per session. On the training day, two identical objects were introduced, and mice were allowed to explore for five minutes. After a one-hour delay, one object was replaced with a novel one. The videos were analysed using CleverSys software stereotypic event "Sniffing" module. Objects were manually outlined with the polygon tool. An interaction with an object was recorded when the mouse's nose was within 5 mm of the object. The novelty preference was determined by calculating the proportion of time spent exploring the novel object relative to the total exploration time of both objects, with a recognition index chance level of 50%.

Elevated plus maze

For cohort 1, EPM was administered to behaviourally naïve animals, while in the for cohort 2, it was conducted after OF and NOR tests. In both cases, mice were placed in the closed arm of the arena (65 x 65 x 55 cm, elevated 40 cm) under full overhead lighting (500 lux) and allowed to explore for five minutes. The arena was divided into closed, middle, and open areas for analysis with CleverSys software. The number of head dips and stretch-attend postures was recorded using BORIS software, and testing accuracy was compared with the results of an independent scorer.

Prepulse inhibition

Like NOR, PPI was only conducted in cohort 2. We used an acoustic startle chamber (SR-LAB, San Diego Instruments, San Diego, CA, USA) with a cylindrical Plexiglas enclosure horizontally mounted on a mobile platform within a sound-proofed isolation chamber. A high-frequency loudspeaker positioned above the enclosure emitted continuous background noise at 65 dB, along with the experimental acoustic stimuli. The startle response was recorded by converting Plexiglas enclosure vibrations into millivolt signals using a piezoelectric unit.

Each session started with a five-minute acclimatisation period to the 65 dB background noise, followed by five startle-alone trials at 120 dB to ensure habituation. Mice then received 10 prepulse stimuli at 3, 6, and 12 dB above background, each preceding a 120 dB pulse in a pseudo-randomised order, interspersed with 10 no-stimulus trials and 10 startle-alone trials. The session concluded with five final startle-alone pulses. The inter-trial interval was randomised

between 9-15 seconds to prevent expectation-based modulation of the startle response. %PPI was calculated for each prepulse using the formula: $\%PPI = \frac{pulse\ alone\ (mV_{Max}) - pulse\ with\ prepulse\ (mV_{Max})}{pulse\ alone\ (mV_{Max})}$.

Statistical procedure for behavioural outcome measures

All statistical analyses were conducted using Python 3.11.7, using relevant libraries such as SciPy and statsmodels. For both studies, the Shapiro-Wilk test was used to assess the normality of data distributions, while Levene's test was used to evaluate homogeneity of variances. When either assumption of normality or equal variance was violated, Kruskal-Wallis test was used, followed by Dunn's test for post hoc pairwise comparisons with Bonferroni correction for multiple testing where applicable. For datasets meeting parametric assumptions, different approaches were used based on the study design. For cohort 1, a two-way ANOVA was performed to analyse the effect of sex, genotype and sex-by-genotype interaction, followed by Tukey's test for post hoc comparisons. Bonferroni correction was applied to adjust for multiple comparisons. Due to the relatively small sample size (n = 38) in cohort 2, sex-by-genotype interactions were not analysed. Instead, Student's *t*-test was used for comparisons between groups.

To balance statistical rigor with preserving power in exploratory contexts, behavioural measures were not universally corrected for multiplicity. Instead, robustness was inferred through replication across independent cohorts and broad phenotypic consistency. The threshold for statistical significance was set at $p < 0.05$. Individual mice served as the experimental units in all analyses.

Code availability

Data and code to reproduce figures will be added to https://github.com/hannalemmik upon publication. The MRI processing code is available upon request from Eugene Kim.

Data availability

Behaviour videos will be added to figshare, and MRI data will be added to openneuro. The intermediary analysis files will be added to github at https://github.com/hannalemmik.

Acknowledgements

We thank Bao Lu and Craig Gerard for providing the *C3ar1* knockout mice, Dr Marija M. Petrinovic for providing prepulse inhibition testing equipment and KCL Biological Service Unit staff for animal care. This work was funded by the MRC grant "Complement C3aR in adolescent synaptic pruning and risk for anxiety" (MR/W004607/1). Hanna Lemmik was funded by the Wellcome Trust as part of the "Neuro-Immune Interactions in Health & Disease" Wellcome Trust PhD Programme (218452/Z/19/Z).

Author contributions

HL - writing - original draft, writing - review & editing, conceptualization, methodology, software, formal analysis, data curation, investigation, visualization, funding acquisition; EK - methodology, software, formal analysis, investigation, data curation, writing - review & editing, visualization, funding acquisition; EM - methodology, software, investigation, writing - review & editing; DM - validation, methodology, investigation; MB - software, formal analysis, data curation, visualization; ZL - investigation, validation; DA - investigation, Esther - investigation; MES - funding acquisition; WZ - resources, supervision; AI - resources, supervision; DC - writing - original draft, writing - review & editing, supervision, project administration, funding acquisition, conceptualization, methodology; LW - writing - original draft, writing - review & editing, supervision, funding acquisition, conceptualization, methodology.

References

Avants, Brian B., Nicholas J. Tustison, Gang Song, Philip A. Cook, Arno Klein, and James C. Gee. 2011. "A Reproducible Evaluation of ANTs Similarity Metric Performance in Brain Image Registration." *NeuroImage* 54 (3): 2033–44.

Bailey, Kathleen R., Nathan R. Rustay, and Jacqueline N. Crawley. 2006. "Behavioral Phenotyping of Transgenic and Knockout Mice: Practical Concerns and Potential Pitfalls." *ILAR Journal* 47 (2): 124–31.

Bassett, Danielle S., Edward T. Bullmore, Andreas Meyer-Lindenberg, José A. Apud, Daniel R. Weinberger, and Richard Coppola. 2009. "Cognitive Fitness of Cost-Efficient Brain Functional Networks." *Proceedings of the National Academy of Sciences of the United States of America* 106 (28): 11747–52.

Baum, Matthew L., Daniel K. Wilton, Rachel G. Fox, Alanna Carey, Yu-Han H. Hsu, Ruilong Hu, Henna J. Jäntti, et al. 2024. "CSMD1 Regulates Brain Complement Activity and Circuit Development." *Brain, Behavior, and Immunity*, March.

Bénard, Magalie, Emilie Raoult, David Vaudry, Jérome Leprince, Anthony Falluel-Morel, Bruno J. Gonzalez, Ludovic Galas, Hubert Vaudry, and Marc Fontaine. 2008. "Role of Complement Anaphylatoxin Receptors (C3aR, C5aR) in the Development of the Rat Cerebellum." *Molecular Immunology* 45 (14): 3767–74.

Berlot, Rok, Claudia Metzler-Baddeley, M. Arfan Ikram, Derek K. Jones, and Michael J. O'Sullivan. 2016. "Global Efficiency of Structural Networks Mediates Cognitive Control in Mild Cognitive Impairment." *Frontiers in Aging Neuroscience* 8 (December): 292.

Brouwer, Rachel M., René C. W. Mandl, Hugo G. Schnack, Inge L. C. van Soelen, G. Caroline van Baal, Jiska S. Peper, René S. Kahn, Dorret I. Boomsma, and H. E. Hulshoff Pol. 2012. "White Matter Development in Early Puberty: A Longitudinal Volumetric and Diffusion Tensor Imaging Twin Study." *PloS One* 7 (4): e32316.

Brust, Vera, Philipp M. Schindler, and Lars Lewejohann. 2015. "Lifetime Development of Behavioural Phenotype in the House Mouse (Mus Musculus)." *Frontiers in Zoology* 12 Suppl 1 (S1): S17.

Bullmore, Ed, and Olaf Sporns. 2009. "Complex Brain Networks: Graph Theoretical Analysis of Structural and Functional Systems." *Nature Reviews. Neuroscience* 10 (3): 186–98.

Byrne, Jonah F., Colm Healy, Melanie Föcking, Meike Heurich, Subash Raj Susai, David Mongan, Kieran Wynne, et al. 2024. "Plasma Complement and Coagulation Proteins as Prognostic Factors of Negative Symptoms: An Analysis of the NAPLS 2 and 3 Studies." *Brain, Behavior, and Immunity* 119 (July): 188–96.

Cai, Lin, Qi Dong, and Haijing Niu. 2018. "The Development of Functional Network Organization in Early Childhood and Early Adolescence: A Resting-State FNIRS Study." *Developmental Cognitive Neuroscience* 30 (April): 223–35.

Caseras, Xavier, Emily Simmonds, Antonio F. Pardiñas, Richard Anney, Sophie E. Legge, James T. R. Walters, Neil A. Harrison, Michael C. O'Donovan, and Valentina Escott-Price. 2024. "Common Risk Alleles for Schizophrenia within the

Major Histocompatibility Complex Predict White Matter Microstructure." *Translational Psychiatry* 14 (1): 194.

Chahboune, Halima, Laura R. Ment, William B. Stewart, Xiaoxian Ma, Douglas L. Rothman, and Fahmeed Hyder. 2007. "Neurodevelopment of C57B/L6 Mouse Brain Assessed by in Vivo Diffusion Tensor Imaging." *NMR in Biomedicine* 20 (3): 375–82.

Chan, Shi Yu, Eamon Fitzgerald, Zhen Ming Ngoh, Janice Lee, Jasmine Chuah, Joanne S. M. Chia, Marielle V. Fortier, et al. 2024. "Examining the Associations between Microglia Genetic Capacity, Early Life Exposures and White Matter Development at the Level of the Individual." *Brain, Behavior, and Immunity* 119 (July): 781–91.

Chaplin, Hugh, Jr. 2020. "Review: The Burgeoning History of the Complement System 1888-2005." *Immunohematology / American Red Cross* 21 (3): 85–93.

Chew, Gabriel, and Enrico Petretto. 2019. "Transcriptional Networks of Microglia in Alzheimer's Disease and Insights into Pathogenesis." *Genes* 10 (10). https://doi.org/10.3390/genes10100798.

Coulthard, L. G., O. A. Hawksworth, J. Conroy, J. D. Lee, and T. M. Woodruff. 2018. "Complement C3a Receptor Modulates Embryonic Neural Progenitor Cell Proliferation and Cognitive Performance." *Molecular Immunology* 101 (September): 176–81.

Courten-Myers, G. M. de. 1999. "The Human Cerebral Cortex: Gender Differences in Structure and Function." *Journal of Neuropathology and Experimental Neurology* 58 (3): 217–26.

Coutinho, Joana Fernandes, Sara Veiga Fernandesl, José Miguel Soares, Liliana Maia, Óscar Filipe Gonçalves, and Adriana Sampaio. 2016. "Default Mode Network Dissociation in Depressive and Anxiety States." *Brain Imaging and Behavior* 10 (1): 147–57.

Crawley, J. N. 2007. "What's Wrong with My Mouse?: Behavioral Phenotyping of Transgenic and Knockout Mice." (2nd ed.). *John Wiley & Sons Inc.*

Crews, David, David Rushworth, Francisco Gonzalez-Lima, and Sonoko Ogawa. 2009. "Litter Environment Affects Behavior and Brain Metabolic Activity of Adult Knockout Mice." *Frontiers in Behavioral Neuroscience* 3 (August): 12.

1025 Crider, A., T. Feng, C. D. Pandya, T. Davis, A. Nair, A. O. Ahmed, B. Baban, D.
1026 Turecki, and A. Pillai. 2018. "Complement Component 3a Receptor Deficiency
1027 Attenuates Chronic Stress-Induced Monocyte Infiltration and Depressive-like
1028 Behavior." *Brain, Behavior, and Immunity* 70 (May): 246–56.

1029 Deivasigamani, Senthilkumar, Mariya T. Miteva, Silvia Natale, Daniel Gutierrez-
1030 Barragan, Bernadette Basilico, Silvia Di Angelantonio, Laetitia Weinhard, et al. 2023.
1031 "Microglia Complement Signaling Promotes Neuronal Elimination and Normal
1032 Brain Functional Connectivity." *Cerebral Cortex* 33 (21): 10750–60.

1033 El-Brolosy, Mohamed A., Zacharias Kontarakis, Andrea Rossi, Carsten Kuenne,
1034 Stefan Günther, Nana Fukuda, Khrievono Kikhi, et al. 2019. "Genetic
1035 Compensation Triggered by Mutant MRNA Degradation." *Nature* 568 (7751):
1036 193–97.

1037 El-Brolosy, Mohamed A., and Didier Y. R. Stainier. 2017. "Genetic Compensation:
1038 A Phenomenon in Search of Mechanisms." *PLoS Genetics* 13 (7): e1006780.

1039 Ellegood, Jacob, Yohan Yee, Travis M. Kerr, Christopher L. Muller, Randy D.
1040 Blakely, R. Mark Henkelman, Jeremy Veenstra-VanderWeele, and Jason P. Lerch.
1041 2018. "Analysis of Neuroanatomical Differences in Mice with Genetically Modified
1042 Serotonin Transporters Assessed by Structural Magnetic Resonance Imaging."
1043 *Molecular Autism* 9 (1): 24.

1044 Falangola, Maria Fatima, Siddhartha Dhiman, Joshua Voltin, and Jens H. Jensen.
1045 2023. "Quantitative Microglia Morphological Features Correlate with Diffusion
1046 MRI in 2-Month-Old 3xTg-AD Mice." *Magnetic Resonance Imaging* 103
1047 (November): 8–17.

1048 Filipello, Fabia, Raffaella Morini, Irene Corradini, Valerio Zerbi, Alice Canzi,
1049 Bernadeta Michalski, Marco Erreni, et al. 2018. "The Microglial Innate Immune
1050 Receptor TREM2 Is Required for Synapse Elimination and Normal Brain
1051 Connectivity." *Immunity* 48 (5): 979-991.e8.

1052 Fitch, W. M., and W. R. Atchley. 1985. "Evolution in Inbred Strains of Mice
1053 Appears Rapid." *Science (New York, N.Y.)* 228 (4704): 1169–75.

1054 Forlim, Caroline Garcia, Leonie Klock, Jürgen Gallinat, and Simone Kühn. 2024.
1055 "Altered Resting-State Functional Connectivity in a Thalamo-Cortico-Cerebellar
1056 Network in Patients with Schizophrenia." *Scientific Reports* 14 (1): 26284.

Ge, Tong-Qi, Pei-Pei Guan, and Pu Wang. 2024. "Complement 3a Induces the Synapse Loss via C3aR in Mitochondria-Dependent NLRP3 Activating Mechanisms during the Development and Progression of Alzheimer's Disease." *Neuroscience and Biobehavioral Reviews* 165 (105868): 105868.

Gedam, Manasee, Michele M. Comerota, Nicholas E. Propson, Tao Chen, Feng Jin, Meng C. Wang, and Hui Zheng. 2023. "Complement C3aR Depletion Reverses HIF-1α-Induced Metabolic Impairment and Enhances Microglial Response to Aβ Pathology." *The Journal of Clinical Investigation* 133 (12).

Geng, Haiyang, Xuebing Li, Jie Chen, Xinying Li, and Ruolei Gu. 2015. "Decreased Intra- and Inter-Salience Network Functional Connectivity Is Related to Trait Anxiety in Adolescents." *Frontiers in Behavioral Neuroscience* 9: 350.

Girardi, Guillermina, Joshua J. Lingo, Sherry D. Fleming, and Jean F. Regal. 2020. "Essential Role of Complement in Pregnancy: From Implantation to Parturition and Beyond." *Frontiers in Immunology* 11 (July): 1681.

Gnanaguru, Gopalan, Steven J. Tabor, Gracia M. Bonilla, Ruslan Sadreyev, Kentaro Yuda, Jörg Köhl, and Kip M. Connor. 2023. "Microglia Refine Developing Retinal Astrocytic and Vascular Networks through the Complement C3/C3aR Axis." *Development* 150 (5).

Gorski, R. A., J. H. Gordon, J. E. Shryne, and A. M. Southam. 1978. "Evidence for a Morphological Sex Difference within the Medial Preoptic Area of the Rat Brain." *Brain Research* 148 (2): 333–46.

Grandjean, J., C. Canella, C. Anckaerts, C. Ayrancı, S. Bougacha, T. Bienert, D. Buehlmann, et al. 2020. "Common Functional Networks in the Mouse Brain Revealed by Multi-Centre Resting-State FMRI Analysis." *NeuroImage* 205 (January).

Grandjean, Joanes, Aileen Schroeter, Imene Batata, and Markus Rudin. 2014. "Optimization of Anesthesia Protocol for Resting-State FMRI in Mice Based on Differential Effects of Anesthetics on Functional Connectivity Patterns." *NeuroImage* 102 Pt 2 (November): 838–47.

Gretenkord, Sabine, Johanna K. Kostka, Henrike Hartung, Katja Watznauer, David Fleck, Angélica Minier-Toribio, Marc Spehr, and Ileana L. Hanganu-Opatz. 2019. "Coordinated Electrical Activity in the Olfactory Bulb Gates the Oscillatory

Entrainment of Entorhinal Networks in Neonatal Mice." *PLoS Biology* 17 (1): e2006994.

Guma, Elisa, Antoine Beauchamp, Siyuan Liu, Elizabeth Levitis, Jacob Ellegood, Linh Pham, Rogier B. Mars, Armin Raznahan, and Jason P. Lerch. 2024. "Comparative Neuroimaging of Sex Differences in Human and Mouse Brain Anatomy." *ELife* 13 (March).

Guma, Elisa, Maude Bordeleau, Fernando González Ibáñez, Katherine Picard, Emily Snook, Gabriel Desrosiers-Grégoire, Shoshana Spring, et al. 2022. "Differential Effects of Early or Late Exposure to Prenatal Maternal Immune Activation on Mouse Embryonic Neurodevelopment." *Proceedings of the National Academy of Sciences of the United States of America* 119 (12): e2114545119.

Hadley, Jennifer Ann, Nina Vanessa Kraguljac, David Matthew White, Lawrence Ver Hoef, Janell Tabora, and Adrienne Carol Lahti. 2016. "Change in Brain Network Topology as a Function of Treatment Response in Schizophrenia: A Longitudinal Resting-State FMRI Study Using Graph Theory." *Npj Schizophrenia* 2 (1): 16014.

Hagmann, P., O. Sporns, N. Madan, L. Cammoun, R. Pienaar, V. J. Wedeen, R. Meuli, J-P Thiran, and P. E. Grant. 2010. "White Matter Maturation Reshapes Structural Connectivity in the Late Developing Human Brain." *Proceedings of the National Academy of Sciences of the United States of America* 107 (44): 19067–72.

Hammond, Timothy R., Connor Dufort, Lasse Dissing-Olesen, Stefanie Giera, Adam Young, Alec Wysoker, Alec J. Walker, et al. 2019. "Single-Cell RNA Sequencing of Microglia throughout the Mouse Lifespan and in the Injured Brain Reveals Complex Cell-State Changes." *Immunity* 50 (1): 253-271.e6.

Hauser, Alexander S., Misty M. Attwood, Mathias Rask-Andersen, Helgi B. Schiöth, and David E. Gloriam. 2017. "Trends in GPCR Drug Discovery: New Agents, Targets and Indications." *Nature Reviews. Drug Discovery* 16 (12): 829–42.

Hawkins, R., A. S. Shatil, L. Lee, A. Sengupta, L. Zhang, S. Morrow, and R. I. Aviv. 2020. "Reduced Global Efficiency and Random Network Features in Patients with Relapsing-Remitting Multiple Sclerosis with Cognitive Impairment." *AJNR. American Journal of Neuroradiology* 41 (3): 449–55.

Hikishima, Keigo, Tomokazu Tsurugizawa, Kazumi Kasahara, Ryo Takagi, Kiyoshi Yoshinaka, and Naotaka Nitta. 2023. "Brain-Wide Mapping of Resting-State

Networks in Mice Using High-Frame Rate Functional Ultrasound." *NeuroImage* 279 (120297): 120297.

Hines, M., L. S. Allen, and R. A. Gorski. 1992. "Sex Differences in Subregions of the Medial Nucleus of the Amygdala and the Bed Nucleus of the Stria Terminalis of the Rat." *Brain Research* 579 (2): 321–26.

Holmdahl, Rikard, and Bernard Malissen. 2012. "The Need for Littermate Controls." *European Journal of Immunology* 42 (1): 45–47.

Hong, Soyon, Victoria F. Beja-Glasser, Bianca M. Nfonoyim, Arnaud Frouin, Shaomin Li, Saranya Ramakrishnan, Katherine M. Merry, et al. 2016. "Complement and Microglia Mediate Early Synapse Loss in Alzheimer Mouse Models." *Science* 352 (6286): 712–16.

Howes, Oliver D., Bernard R. Bukala, and Katherine Beck. 2024. "Schizophrenia: From Neurochemistry to Circuits, Symptoms and Treatments." *Nature Reviews. Neurology* 20 (1): 22–35.

Humbles, Alison A., Bao Lu, Christy A. Nilsson, Craig Lilly, Elliot Israel, Yuko Fujiwara, Norma P. Gerard, and Craig Gerard. 2000. "A Role for the C3a Anaphylatoxin Receptor in the Effector Phase of Asthma." *Nature* 406 (6799): 998–1001.

Jenkinson, Mark, Christian F. Beckmann, Timothy E. J. Behrens, Mark W. Woolrich, and Stephen M. Smith. 2012. "FSL." *NeuroImage* 62 (2): 782–90.

Jiang, Weixiong, Zhen Zhou, Guoshi Li, Weiyan Yin, Zhengwang Wu, Li Wang, Maryam Ghanbari, et al. 2023. "Mapping the Evolution of Regional Brain Network Efficiency and Its Association with Cognitive Abilities during the First Twenty-Eight Months of Life." *Developmental Cognitive Neuroscience* 63 (101284): 101284.

Jiménez, Jessica A., and Mark J. Zylka. 2021. "Controlling Litter Effects to Enhance Rigor and Reproducibility with Rodent Models of Neurodevelopmental Disorders." *Journal of Neurodevelopmental Disorders* 13 (1): 2.

Kalbassi, Shireene, Sven O. Bachmann, Ellen Cross, Victoria H. Roberton, and Stéphane J. Baudouin. 2017. "Male and Female Mice Lacking Neuroligin-3 Modify the Behavior of Their Wild-Type Littermates." *ENeuro* 4 (4).

Kiani Shabestari, Sepideh, Samuel Morabito, Emma Pascal Danhash, Amanda McQuade, Jessica Ramirez Sanchez, Emily Miyoshi, Jean Paul Chadarevian, et al. 2022. "Absence of Microglia Promotes Diverse Pathologies and Early Lethality in Alzheimer's Disease Mice." *Cell Reports* 39 (11): 110961.

Kielar, Catherine, Stephen J. Sawiak, Paloma Navarro Negredo, Desmond H. Y. Tse, and A. Jennifer Morton. 2012. "Tensor-Based Morphometry and Stereology Reveal Brain Pathology in the Complexin1 Knockout Mouse." *PloS One* 7 (2): e32636.

Kim, Eugene, Ines Carreira Figueiredo, Camilla Simmons, Karen Randall, Loreto Rojo Gonzalez, Tobias Wood, Brigida Ranieri, et al. 2023. "Mapping Acute Neuroinflammation in Vivo with Diffusion-MRI in Rats given a Systemic Lipopolysaccharide Challenge." *Brain, Behavior, and Immunity* 113 (July): 289–301.

Koenis, Marinka M. G., Rachel M. Brouwer, Suzanne C. Swagerman, Inge L. C. van Soelen, Dorret I. Boomsma, and Hilleke E. Hulshoff Pol. 2018. "Association between Structural Brain Network Efficiency and Intelligence Increases during Adolescence." *Human Brain Mapping* 39 (2): 822–36.

Kunz, Natalia, and Claudia Kemper. 2021. "Complement Has Brains-Do Intracellular Complement and Immunometabolism Cooperate in Tissue Homeostasis and Behavior?" *Frontiers in Immunology* 12 (February): 629986.

Lerch, Jason P., Lisa Gazdzinski, Jurgen Germann, John G. Sled, R. Mark Henkelman, and Brian J. Nieman. 2012. "Wanted Dead or Alive? The Tradeoff between in-Vivo versus Ex-Vivo MR Brain Imaging in the Mouse." *Frontiers in Neuroinformatics* 0 (March): 6.

Li, Chenchen, Bo Liu, Jingyi Xu, Bin Jing, Lijie Guo, Liyong Wang, Milin Wang, et al. 2023. "Phloretin Decreases Microglia-Mediated Synaptic Engulfment to Prevent Chronic Mild Stress-Induced Depression-like Behaviors in the MPFC." *Theranostics* 13 (3): 955–72.

Lian, Hong, Li Yang, Allysa Cole, Lu Sun, Angie C-A Chiang, Stephanie W. Fowler, David J. Shim, et al. 2015. "NFκB-Activated Astroglial Release of Complement C3 Compromises Neuronal Morphology and Function Associated with Alzheimer's Disease." *Neuron* 85 (1): 101–15.

Ludewig, Katja, Mark A. Geyer, and Franz X. Vollenweider. 2003. "Deficits in Prepulse Inhibition and Habituation in Never-Medicated, First-Episode Schizophrenia." *Biological Psychiatry* 54 (2): 121–28.

Madeshiya, Amit Kumar, Carl Whitehead, Ashutosh Tripathi, and Anilkumar Pillai. 2022. "C1q Deletion Exacerbates Stress-Induced Learned Helplessness Behavior and Induces Neuroinflammation in Mice." *Translational Psychiatry* 12 (1): 50.

Mamane, Yaël, Chi Chung Chan, Genevieve Lavallee, Nicolas Morin, Li-Jing Xu, Jingqi Huang, Robert Gordon, et al. 2009. "The C3a Anaphylatoxin Receptor Is a Key Mediator of Insulin Resistance and Functions by Modulating Adipose Tissue Macrophage Infiltration and Activation." *Diabetes* 58 (9): 2006–17.

McCarty, Richard. 2017. "Cross-Fostering: Elucidating the Effects of Gene×environment Interactions on Phenotypic Development." *Neuroscience and Biobehavioral Reviews* 73 (February): 219–54.

McCutcheon, Robert A., Tiago Reis Marques, and Oliver D. Howes. 2020. "Schizophrenia-an Overview." *JAMA Psychiatry (Chicago, Ill.)* 77 (2): 201–10.

Mena, Auxiliadora, Juan C. Ruiz-Salas, Andrea Puentes, Inmaculada Dorado, Miguel Ruiz-Veguilla, and Luis G. De la Casa. 2016. "Reduced Prepulse Inhibition as a Biomarker of Schizophrenia." *Frontiers in Behavioral Neuroscience* 10 (October): 202.

Mommert, Susanne, Derya Aslan, Lisanne Ratz, Holger Stark, Ralf Gutzmer, and Thomas Werfel. 2018. "The Anaphylatoxin C3a Receptor Expression on Human M2 Macrophages Is Down-Regulated by Stimulating the Histamine H4 Receptor and the IL-4 Receptor." *Journal of Innate Immunity* 10 (4): 349–62.

Nasseef, Md Taufiq, Gabriel A. Devenyi, Anna E. Mechling, Laura-Adela Harsan, M. Mallar Chakravarty, Brigitte Lina Kieffer, and Emmanuel Darcq. 2018. "Deformation-Based Morphometry MRI Reveals Brain Structural Modifications in Living Mu Opioid Receptor Knockout Mice." *Frontiers in Psychiatry* 9 (December): 643.

O'Connell, Kevin S., Ida E. Sønderby, Oleksandr Frei, Dennis van der Meer, Lavinia Athanasiu, Olav B. Smeland, Dag Alnæs, et al. 2021. "Association between Complement Component 4A Expression, Cognitive Performance and Brain Imaging Measures in UK Biobank." *Psychological Medicine* 52 (15): 1–11.

Olsen, Reid H. J., Jeffrey F. DiBerto, Justin G. English, Alexis M. Glaudin, Brian E. Krumm, Samuel T. Slocum, Tao Che, et al. 2020. "TRUPATH, an Open-Source Biosensor Platform for Interrogating the GPCR Transducerome." *Nature Chemical Biology* 16 (8): 841–49.

Osimo, Emanuele Felice, Katherine Beck, Tiago Reis Marques, and Oliver D. Howes. 2019. "Synaptic Loss in Schizophrenia: A Meta-Analysis and Systematic Review of Synaptic Protein and MRNA Measures." *Molecular Psychiatry* 24 (4): 549–61.

Paus, T., M. Keshavan, and J. N. Giedd. 2008. "Why Do Many Psychiatric Disorders Emerge during Adolescence?" *Nature Reviews. Neuroscience* 9 (12): 947–57.

Piekarski, David J., Natalie M. Zahr, Qingyu Zhao, Uran Ferizi, Kilian M. Pohl, Edith V. Sullivan, and Adolf Pfefferbaum. 2023. "White Matter Microstructural Integrity Continues to Develop from Adolescence to Young Adulthood in Mice and Humans: Same Phenotype, Different Mechanism." *Neuroimage. Reports* 3 (3).

Pintér, O., Zoltan Beda, Z. Csaba, and I. Gerendai. 2007. "Differences in the Onset of Puberty in Selected Inbred Mouse Strains." *Endocrine Abstracts* 14 (April).

Pozo-Rodrigálvarez, Andrea, Roosa Ollaranta, Jenny Skoog, Milos Pekny, and Marcela Pekna. 2021. "Hyperactive Behavior and Altered Brain Morphology in Adult Complement C3a Receptor Deficient Mice." *Frontiers in Immunology* 12 (February): 406.

Qiu, Lily R., Darren J. Fernandes, Kamila U. Szulc-Lerch, Jun Dazai, Brian J. Nieman, Daniel H. Turnbull, Jane A. Foster, Mark R. Palmert, and Jason P. Lerch. 2018. "Mouse MRI Shows Brain Areas Relatively Larger in Males Emerge before Those Larger in Females." *Nature Communications* 9 (1): 1–15.

Quell, Katharina M., Christian M. Karsten, Anna Kordowski, Larissa Nogueira Almeida, Daria Briukhovetska, Anna V. Wiese, Jing Sun, et al. 2017. "Monitoring C3aR Expression Using a Floxed TdTomato-C3aR Reporter Knock-in Mouse." *The Journal of Immunology* 199 (2): 688–706.

Reynolds, Jess E., Melody N. Grohs, Deborah Dewey, and Catherine Lebel. 2019. "Global and Regional White Matter Development in Early Childhood." *NeuroImage* 196 (August): 49–58.

Rodriguez, Pedro, Lauren J. Laskowski, Jean Pierre Pallais, Hailey A. Bock, Natalie G. Cavalco, Emilie I. Anderson, Maggie M. Calkins, et al. 2023. "Functional Profiling of the G Protein-Coupled Receptor C3aR1 Reveals Ligand-Mediated Biased Agonism." *The Journal of Biological Chemistry* 300 (1): 105549.

Rojo, Rocío, Anna Raper, Derya D. Ozdemir, Lucas Lefevre, Kathleen Grabert, Evi Wollscheid-Lengeling, Barry Bradford, et al. 2019. "Deletion of a Csf1r Enhancer Selectively Impacts CSF1R Expression and Development of Tissue Macrophage Populations." *Nature Communications* 10 (1): 3215.

Rubinov, Mikail, and Olaf Sporns. 2010. "Complex Network Measures of Brain Connectivity: Uses and Interpretations." *NeuroImage* 52 (3): 1059–69.

Schimmelpfennig, Jakub, Jan Topczewski, Wojciech Zajkowski, and Kamila Jankowiak-Siuda. 2023. "The Role of the Salience Network in Cognitive and Affective Deficits." *Frontiers in Human Neuroscience* 17 (March): 1133367.

Schizophrenia Working Group of the Psychiatric Genomics Consortium. 2014. "Biological Insights from 108 Schizophrenia-Associated Genetic Loci." *Nature* 511 (7510): 421–27.

Sekar, A., A. R. Bialas, H. de Rivera, A. Davis, T. R. Hammond, Kamitaki N, Tooley K, et al. 2016. "Schizophrenia Risk from Complex Variation of Complement Component 4." *Nature* 530 (7589): 177–83.

Semaan, Sheila J., and Alexander S. Kauffman. 2015. "Daily Successive Changes in Reproductive Gene Expression and Neuronal Activation in the Brains of Pubertal Female Mice." *Molecular and Cellular Endocrinology* 401 (February): 84–97.

Serrano, Maria Elisa, Eugene Kim, Bernard Siow, Da Ma, Loreto Rojo, Camilla Simmons, Darryl Hayward, et al. 2023. "Investigating Brain Alterations in the Dp1Tyb Mouse Model of Down Syndrome - ScienceDirect." *Neurobiology of Disease* 188 (November): 106336.

Sforazzini, Francesco, Adam J. Schwarz, Alberto Galbusera, Angelo Bifone, and Alessandro Gozzi. 2014. "Distributed BOLD and CBV-Weighted Resting-State Networks in the Mouse Brain." *NeuroImage* 87 (February): 403–15.

Smith, Stephen M., Mark Jenkinson, Mark W. Woolrich, Christian F. Beckmann, Timothy E. J. Behrens, Heidi Johansen-Berg, Peter R. Bannister, et al. 2004.

"Advances in Functional and Structural MR Image Analysis and Implementation as FSL." *NeuroImage* 23 Suppl 1 (January): S208-19.

Stevens, Beth, Nicola J. Allen, Luis E. Vazquez, Gareth R. Howell, Karen S. Christopherson, Navid Nouri, Kristina D. Micheva, et al. 2007. "The Classical Complement Cascade Mediates CNS Synapse Elimination." *Cell* 131 (6): 1164–78.

Sun, Rui, Meng-Yu Tang, Dan Yang, Yan-Yi Zhang, Yi-Heng Xu, Yong Qiao, Bin Yu, et al. 2024. "C3aR in the Medial Prefrontal Cortex Modulates the Susceptibility to LPS-Induced Depressive-like Behaviors through Glutamatergic Neuronal Excitability." *Progress in Neurobiology*, April, 102614.

Tabbaa, Manal, Allison Knoll, and Pat Levitt. 2023. "Mouse Population Genetics Phenocopies Heterogeneity of Human Chd8 Haploinsufficiency." *Neuron* 111 (4): 539-556.e5.

Tao, Juan, Jing Zhao, Xiang-Ming Qi, and Yong-Gui Wu. 2021. "Complement-Mediated M2/M1 Macrophage Polarization May Be Involved in Crescent Formation in Lupus Nephritis." *International Immunopharmacology* 101 (Pt A): 108278.

Tasic, Bosiljka, Vilas Menon, Thuc Nghi Nguyen, Tae Kyung Kim, Tim Jarsky, Zizhen Yao, Boaz Levi, et al. 2016. "Adult Mouse Cortical Cell Taxonomy Revealed by Single Cell Transcriptomics." *Nature Neuroscience* 19 (2): 335–46.

Tasic, Bosiljka, Zizhen Yao, Lucas T. Graybuck, Kimberly A. Smith, Thuc Nghi Nguyen, Darren Bertagnolli, Jeff Goldy, et al. 2018. "Shared and Distinct Transcriptomic Cell Types across Neocortical Areas." *Nature* 563 (7729): 72–78.

Thirion, Bertrand, Gaël Varoquaux, Elvis Dohmatob, and Jean-Baptiste Poline. 2014. "Which FMRI Clustering Gives Good Brain Parcellations?" *Frontiers in Neuroscience* 8 (July): 167.

Tillmon, Haven, Breeanne M. Soteros, Liang Shen, Qifei Cong, Mackenna Wollet, Julianne General, Hanna Chin, et al. 2024. "Complement and Microglia Activation Mediate Stress-Induced Synapse Loss in Layer 2/3 of the Medial Prefrontal Cortex in Male Mice." *Nature Communications* 15 (1): 9803.

Tournier, J-Donald, Robert Smith, David Raffelt, Rami Tabbara, Thijs Dhollander, Maximilian Pietsch, Daan Christiaens, Ben Jeurissen, Chun-Hung Yeh, and Alan

Connelly. 2019. “MRtrix3: A Fast, Flexible and Open Software Framework for Medical Image Processing and Visualisation.” *NeuroImage* 202 (116137): 116137.

Tripathi, Ashutosh, Carl Whitehead, Katelyn Surrao, Ananya Pillai, Amit Madeshiya, Yong Li, Hesam Khodadadi, et al. 2021. “Type 1 Interferon Mediates Chronic Stress-Induced Neuroinflammation and Behavioral Deficits via Complement Component 3-Dependent Pathway.” *Molecular Psychiatry* 26 (7): 3043–59.

Vadnie, Chelsea A., Kaitlyn A. Petersen, Lauren A. Eberhardt, Mariah A. Hildebrand, Allison J. Cerwensky, Hui Zhang, Jennifer N. Burns, et al. 2021. “The Suprachiasmatic Nucleus Regulates Anxiety-like Behavior in Mice.” *Frontiers in Neuroscience* 15: 765850.

Valiquette, Vanessa, Elisa Guma, Lani Cupo, Daniel Gallino, Chloe Anastassiadis, Emily Snook, Gabriel A. Devenyi, and M. Mallar Chakravarty. 2023. “Examining Litter Specific Variability in Mice and Its Impact on Neurodevelopmental Studies.” *NeuroImage* 269 (April): 119888.

Vasek, Michael J., Charise Garber, Denise Dorsey, Douglas M. Durrant, Bryan Bollman, Allison Soung, Jinsheng Yu, et al. 2016. “A Complement-Microglial Axis Drives Synapse Loss during Virus-Induced Memory Impairment.” *Nature* 534 (7608): 538–43.

Vita, A., L. De Peri, G. Deste, and E. Sacchetti. 2012. “Progressive Loss of Cortical Gray Matter in Schizophrenia: A Meta-Analysis and Meta-Regression of Longitudinal MRI Studies.” *Translational Psychiatry* 2 (11): e190.

Wang, Quanxin, Song-Lin Ding, Yang Li, Josh Royall, David Feng, Phil Lesnar, Nile Graddis, et al. 2020. “The Allen Mouse Brain Common Coordinate Framework: A 3D Reference Atlas.” *Cell* 181 (4): 936-953.e20.

West, Erin E., and Claudia Kemper. 2023. “Complosome - the Intracellular Complement System.” *Nature Reviews. Nephrology* 19 (7): 426–39.

Westacott, Laura J., Niels Haan, Claudia Evison, Omar Marei, Jeremy Hall, Timothy R. Hughes, Malik Zaben, et al. 2021. “Dissociable Effects of Complement C3 and C3aR on Survival and Morphology of Adult Born Hippocampal Neurons, Pattern Separation, and Cognitive Flexibility in Male Mice.” *Brain, Behavior, and Immunity* 98 (November): 136–50.

Westacott, Laura J., Trevor Humby, Niels Haan, Sophie A. Brain, Emma-Louise Bush, Margarita Toneva, Andreea-Ingrid Baloc, et al. 2022. "Complement C3 and C3aR Mediate Different Aspects of Emotional Behaviours; Relevance to Risk for Psychiatric Disorder." *Brain, Behavior, and Immunity* 99 (January): 70–82.

Westacott, Laura J., and Lawrence S. Wilkinson. 2022. "Complement Dependent Synaptic Reorganisation During Critical Periods of Brain Development and Risk for Psychiatric Disorder." *Frontiers in Neuroscience* 16 (May): 840266.

Wood, Tobias C., Camilla Simmons, Samuel A. Hurley, Anthony C. Vernon, Joel Torres, Flavio Dell'Acqua, Steve C. R. Williams, and Diana Cash. 2016. "Whole-Brain Ex-Vivo Quantitative MRI of the Cuprizone Mouse Model." *PeerJ* 4 (November): e2632.

Yilmaz, Melis, Esra Yalcin, Jessy Presumey, Ernest Aw, Minghe Ma, Christopher W. Whelan, Beth Stevens, Steven A. McCarroll, and Michael C. Carroll. 2021. "Overexpression of Schizophrenia Susceptibility Factor Human Complement C4A Promotes Excessive Synaptic Loss and Behavioral Changes in Mice." *Nature Neuroscience* 24 (2): 214–24.

Zalesky, Andrew, Alex Fornito, and Edward T. Bullmore. 2010. "Network-Based Statistic: Identifying Differences in Brain Networks." *NeuroImage* 53 (4): 1197–1207.

Zalesky, Andrew, Alex Fornito, Ian H. Harding, Luca Cocchi, Murat Yücel, Christos Pantelis, and Edward T. Bullmore. 2010. "Whole-Brain Anatomical Networks: Does the Choice of Nodes Matter?" *NeuroImage* 50 (3): 970–83.

Zhan, Y., R. C. Paolicelli, F. Sforazzini, L. Weinhard, G. Bolasco, F. Pagani, A. I. Vyssotski, et al. 2014. "Deficient Neuron-Microglia Signaling Results in Impaired Functional Brain Connectivity and Social Behavior." *Nature Neuroscience* 17 (3): 400–406.

Zhang, Man-Man, Min-Xia Guo, Qiu-Ping Zhang, Xue-Qin Chen, Na-Zhi Li, Qing Liu, Jie Cheng, et al. 2022. "IL-1R/C3aR Signaling Regulates Synaptic Pruning in the Prefrontal Cortex of Depression." *Cell & Bioscience* 12 (1): 90.

Zheng, Jingwei, Jia'nan Lu, Shuhao Mei, Haijian Wu, Zeyu Sun, Yuanjian Fang, Shenbin Xu, et al. 2021. "Ceria Nanoparticles Ameliorate White Matter Injury after Intracerebral Hemorrhage: Microglia-Astrocyte Involvement in Remyelination." *Journal of Neuroinflammation* 18 (1): 43.

Zhu, Hongru, Changjian Qiu, Yajing Meng, Minlan Yuan, Yan Zhang, Zhengjia Ren, Yuchen Li, et al. 2017. "Altered Topological Properties of Brain Networks in Social Anxiety Disorder: A Resting-State Functional MRI Study." *Scientific Reports* 7 (1): 43089.

Figures

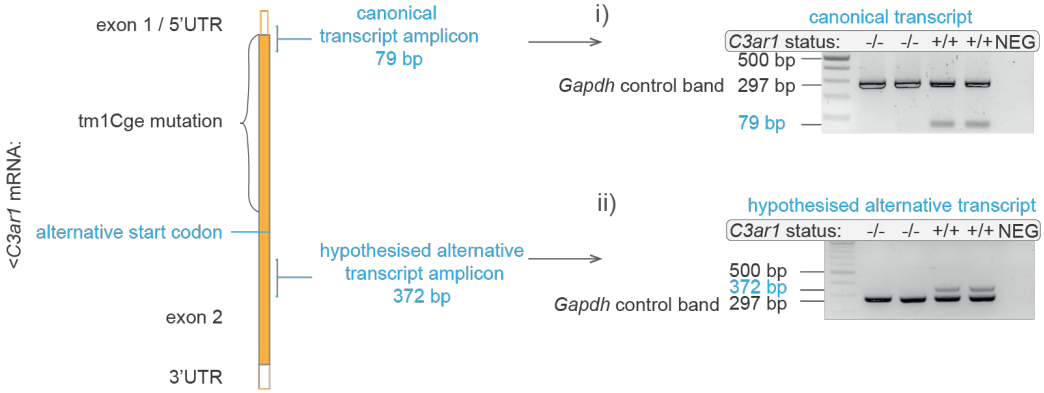

Figure 1 | *C3ar1*^{tm1Cge} mutant does not make *C3ar1* RNA. Schematic shows *C3ar1* mRNA with its only protein coding exon and the design of the 79 bp PCR amplicon which targets an exon-1/5'UTR-exon-2 junction of the canonical C3ar1+/+ transcript. Also shown is another 372 bp amplicon which targets a region downstream of the deletion and after an alternative start codon. The start of exon 2 is deleted in *C3ar1*$^{-/-}$ mice, so PCR should result in no amplification. Similarly, if no alternative transcript is made, there should be no amplification. **(i-ii)** Gel images show PCR products of cDNA from bone-marrow derived interleukin 4 (IL4)-induced M2-like macrophages. Each sample well has a 297 bp Glyceraldehyde 3-phosphate dehydrogenase (*Gapdh*) control band. NEG: no reverse transcriptase negative control. **i)** canonical transcript, **ii)** hypothesised alternative transcript. -/- = *C3ar1*$^{-/-}$, +/+ = *C3ar1*$^{+/+}$.

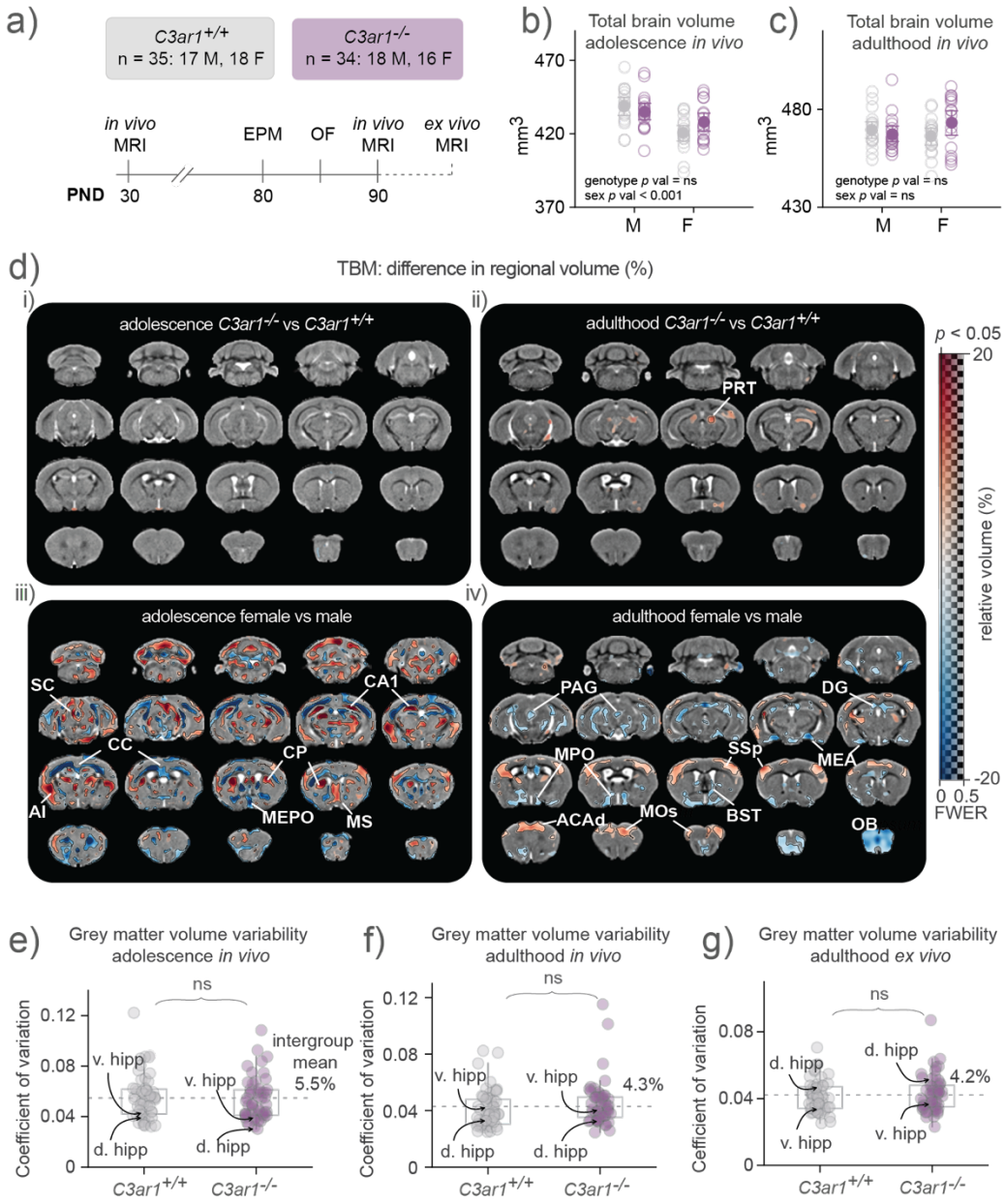
a)
C3ar1+/+
n = 35: 17 M, 18 F
C3ar1-/-
n = 34: 18 M, 16 F
in vivo MRI
EPM
OF
in vivo MRI
ex vivo MRI
PND 30
80
90
b)
Total brain volume adolescence in vivo
mm3
470
420
370
genotype p val = ns
sex p val < 0.001
M
F
c)
Total brain volume adulthood in vivo
mm3
480
430
genotype p val = ns
sex p val = ns
M
F
d)
TBM: difference in regional volume (%)
i)
adolescence C3ar1-/- vs C3ar1+/+
ii)
adulthood C3ar1-/- vs C3ar1+/+
PRT
p < 0.05
20
relative volume (%)
-20
0 0.5
FWER
iii)
adolescence female vs male
SC
CA1
CC
CP
AI
MEPO
MS
iv)
adulthood female vs male
PAG
DG
MPO
SSp
MEA
ACAd
MOs
BST
OB
e)
Grey matter volume variability adolescence in vivo
Coefficient of variation
0.12
0.08
0.04
0
ns
intergroup mean 5.5%
v. hipp
d. hipp
C3ar1+/+
C3ar1-/-
f)
Grey matter volume variability adulthood in vivo
Coefficient of variation
0.12
0.08
0.04
0
ns
4.3%
v. hipp
d. hipp
C3ar1+/+
C3ar1-/-
g)
Grey matter volume variability adulthood ex vivo
Coefficient of variation
0.08
0.04
0
ns
4.2%
d. hipp
v. hipp
C3ar1+/+
C3ar1-/-

1392

Figure 2 | Sex but not *C3ar1* status influences regional brain volume. (a) Schematic of the MRI study shown in **(d-g)**. 69 mice were scanned twice *in vivo*; in adolescence at ~ postnatal day (PND) 30 (range 27-31) and at adulthood ~ PND90 (range 81-92), as well as once *ex vivo* after sacrifice after the adulthood scanning session. Behavioural tests were carried out before the adulthood scanning session. EPM = elevated plus maze, OF = open field. **(b)** Total brain volume at PND30. Two-way ANOVA, genotype, sex, genotype * sex, $F_{[1,65]}$ = 0.35, 16.72, 3.26, p = 0.56, <0.001, 0.76. **(c)** PND90, two-way ANOVA, genotype, sex, genotype * sex, $F_{[1,65]}$ = 0.74, 0.26, 3.33, p = 0.39, 0.61, 0.07. **(b-c)** Data presented as mean ± 95% CI. **(d)** Panels showing relative regional volume changes (%) overlaid on study-specific coronal templates (grey). Red hues signify areas larger in *C3ar1*$^{-/-}$ (**i-ii**) or females (**iii-iv**) and blue hues signify areas larger in *C3ar1*$^{+/+}$ (**i-ii**) or males (**iii-iv**). Transparency of the colour overlay shows the statistical significance, ranging from family wise error (FWE)-corrected p value 0.5 to 0 (transparent to opaque, respectively). Areas where FWE-corrected p value < 0.05 are demarcated with a black line, and where the p value > 0.5 are grey (no overlay), meaning that in adolescence genotype comparison (**i**), no voxels had a p value < 0.5. The locations of the coronal slices in relation to bregma in the left most column from top: -7.6, -4.6, -1.6, 1.4 mm. *C3ar1*$^{+/+}$ n = 35, 17 males and 18 females; *C3ar1*$^{-/-}$ n = 34, 18 males and 16 females. ACAd = dorsal anterior cingulate cortex, AI = agranular insular cortex, BST = bed nucleus of stria terminalis, CA = cornu ammonis, CP = caudoputamen, DG = dentate gyrus, MEA = medial amygdala, MEPO = medial preoptic nucleus, MOs = secondary motor cortex (MOs), MPO = medial preoptic area, MS = medial septum, OB = olfactory bulb, PAG = periaqueductal grey, PRT = pretectal area, SC = superior colliculus, SSp = primary somatosensory cortex. **(e)** Coefficient of variation (CV) in adolescence *in vivo* for 72 regional volumes across all animals in the experiment. **(f)** CV in adulthood *in vivo*. **(g)** CV in adulthood *ex vivo*. **(e-g)** Data are shown with quartiles and whiskers show the extent of the distribution. Dotted line shows the intergroup mean excluding cerebrospinal fluid (CSF) areas. Kruskal Wallis p values, all ns. D. hipp = dorsal hippocampus, v. hipp = ventral hippocampus.

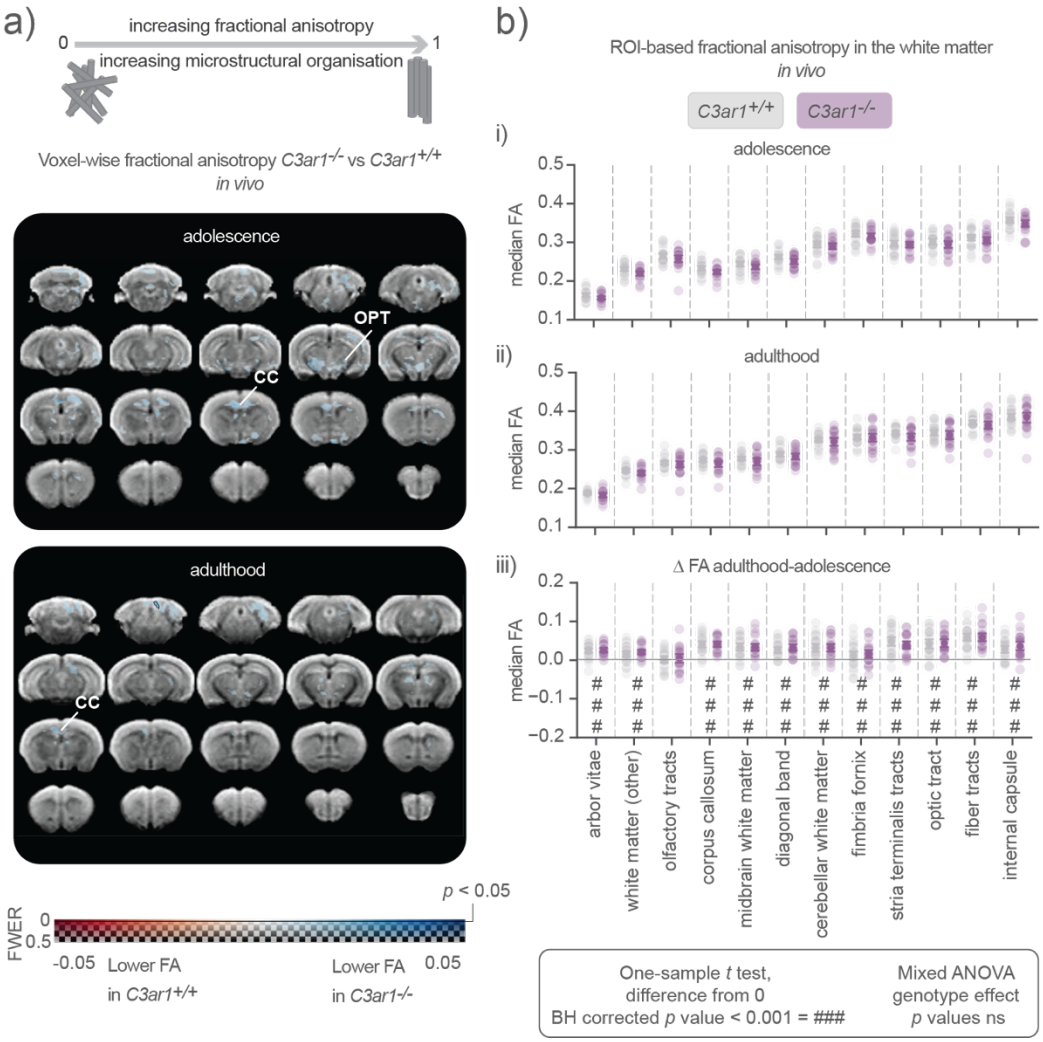

Figure 3 | Fractional anisotropy does not depend on *C3ar1* status but increases with age. (a) Panels showing voxel-wise fractional anisotropy analysis in adolescence (top) and adulthood (bottom) corrected for FWE. There are no significant voxels (no black contour) where genotype effect is significant ($p < 0.05$). CC = corpus callosum, OPT = optic tract. **(b)** *In vivo* ROI-based median fractional anisotropy (FA) values in white matter regions for **(i)** adolescence, **(ii)** adulthood and **(iii)** change over time (adulthood – adolescence). Two-sided one-sample *t* test (difference from 0) *p* values that were adjusted with Benjamini-Hochberg (BH) procedure (### *p* value < 0.001). (**b-i-iii**) Mixed ANOVA with genotype and genotype-by-region interaction effects, all ns. Data are presented as mean ± 95% CI.

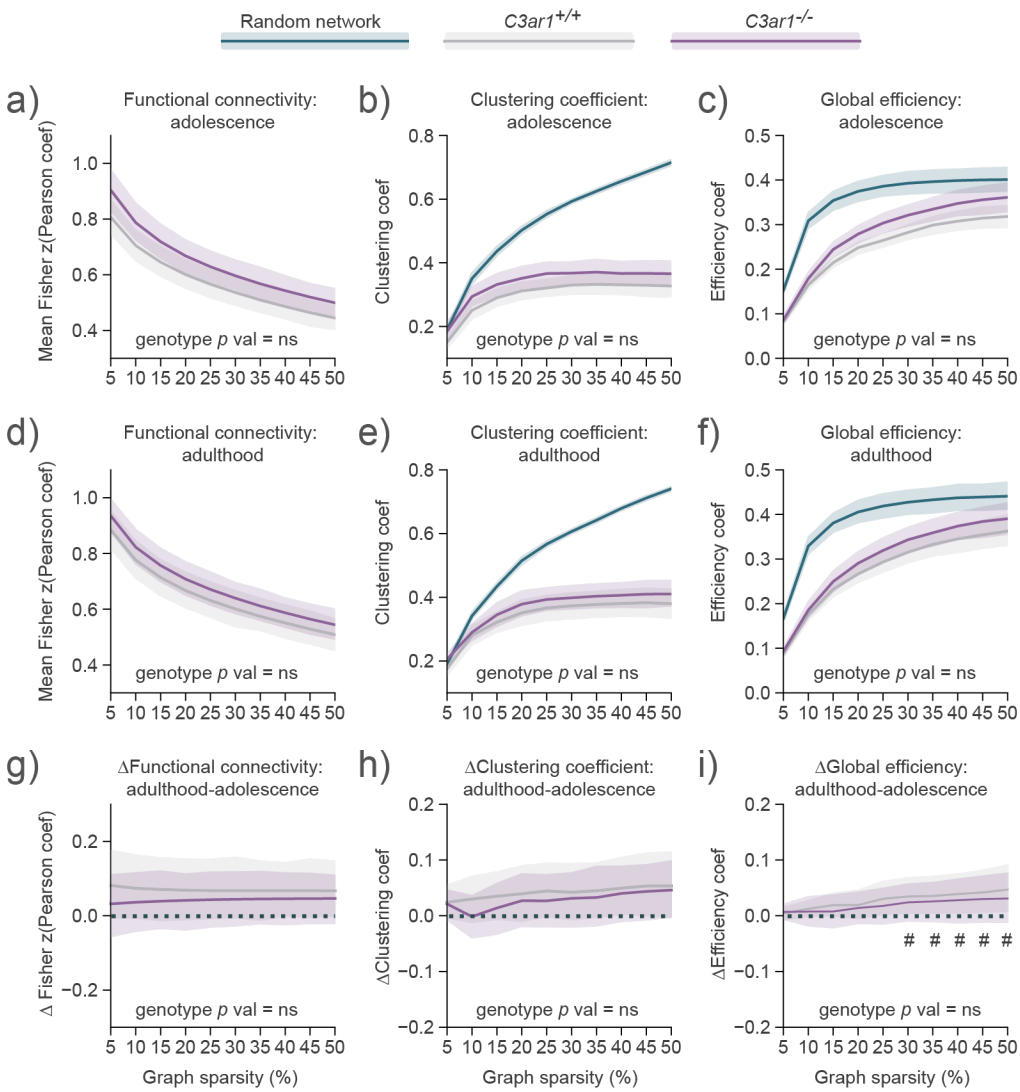

Figure 4 | Global functional connectivity is not changed in *C3ar1*-deficient mice. FC, clustering coefficient and global efficiency at decreasing graph sparsity levels in adolescence **(a-c)**, and adulthood **(d-f)**, and change over time **(g-i)**. **(a-i)** Statistical significance was determined with sexes combined using AUC permutation testing (10,000 iterations) and the resulting *p* values were corrected for multiplicity with the Benjamini-Hochberg method (n = 3 tests per outcome measure). PND30: *C3ar1*$^{+/+}$ n = 32 (15 males, 17 females); *C3ar1*$^{-/-}$ n = 32 (18 males, 14 females); PND90: *C3ar1*$^{+/+}$ n = 33 (16 males, 17 females) and *C3ar1*$^{-/-}$ n = 32 (17 males, 15 females); change: *C3ar1*$^{+/+}$ n = 30 (14 males and 16 females); *C3ar1*$^{-/-}$ n = 31 (17 males and 14 females). Data are shown as mean ± 95% CI. **(g-i)** Two-sided one-sample *t* tests (difference from 0) for global connectivity changes at each sparsity level with genotypes combined, corrected using the Benjamini-Hochberg procedure (n = 10 sparsity levels), # = adjusted *p* value < 0.05.

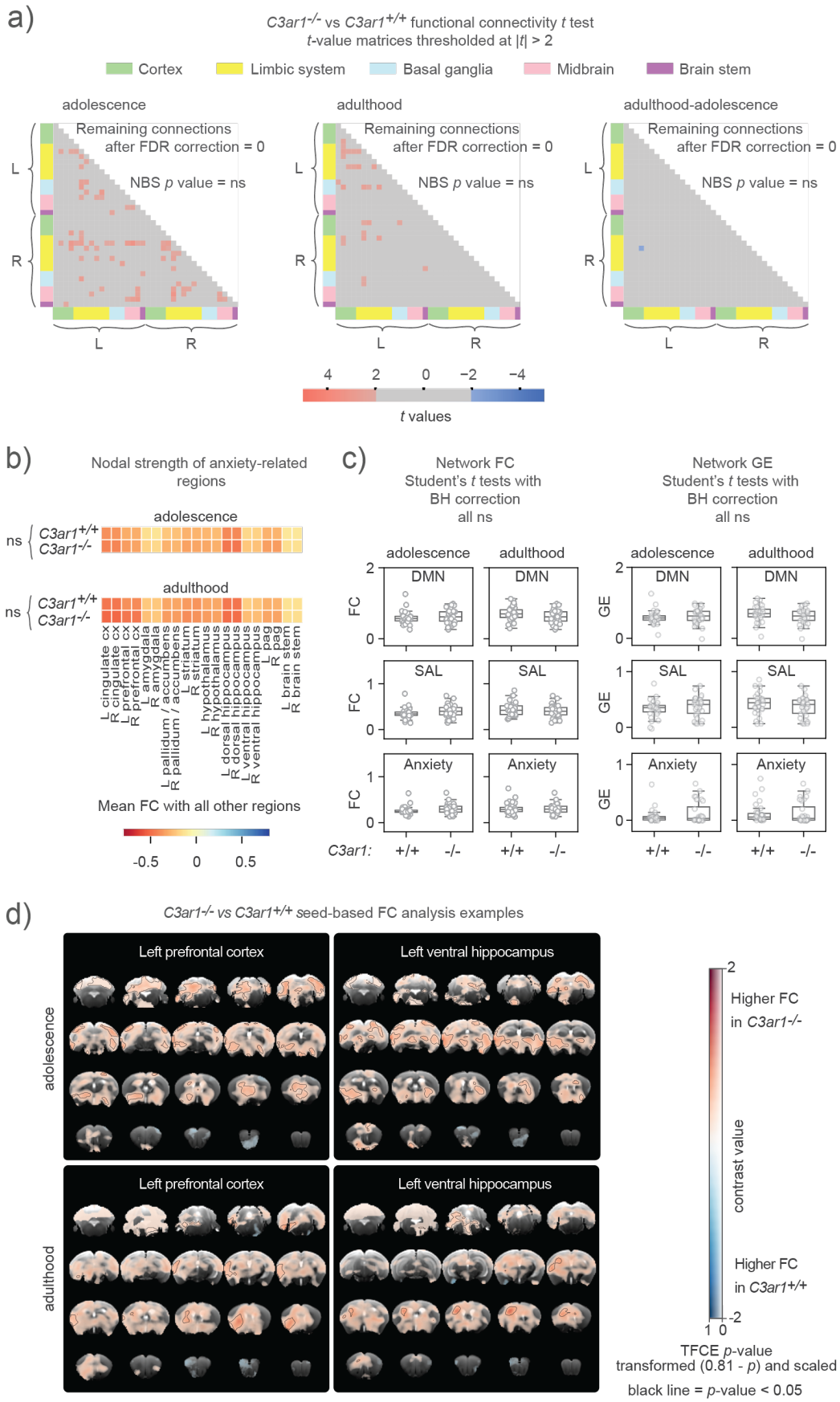

Figure 5 | *C3ar1*-deficiency has no detectable effects on functional brain networks. (a) Thresholded adjacency matrices comparing *C3ar1*$^{+/+}$ vs *C3ar1*$^{-/-}$

groups where $|t| \geq 2$ in adolescence and adulthood, and the change between time points. No connections with $|t| \geq 2$ remained significant after the false discovery rate (FDR) correction. Additionally, the number of connections in the $|t| \geq 2$ adjacency matrix components were not significant when assessed using network-based statistics (NBS) correction. **(b)** Nodal strength (mean absolute connectivity) of *a priori* anxiety-related seeds (e.g. L cingulate cortex correlation coefficients with all other regions). *P* values were calculated using a mixed ANOVA with between-subjects factor of genotype and within-subjects factor of region. Only the region effect was significant at both time-points (both p values < 0.001, $\eta_p^2 = 0.69$ in adolescence and $\eta_p^2 = 0.73$ in adulthood). **(c)** Mean functional connectivity (FC) and global efficiency (GE). Student's *t* tests within a metric (n = 6) corrected for multiple comparisons using the Benjamini-Hochberg method. DMN = default mode network, SAL = salience network, BH = Benjamini-Hochberg. **(d)** Examples of seed-based FC maps showing voxel-wise group differences between *C3ar1*$^{-/-}$ and *C3ar1*$^{+/+}$ mice (using *t* tests) with seeds placed in the left ventral hippocampus and left prefrontal cortex in adolescence and adulthood datasets. The dual scale bar displays contrast value on the x-axis and threshold free cluster enhancement (TFCE) *p*-values (transformed 0.81-p) on the y-axis. The transformed *p*-values have been re-scaled to range from 0 to 1 for visualisation, with darker colours representing greater statistical significance. Black outlines demarcate regions where TFCE *p*-values are below 0.05.

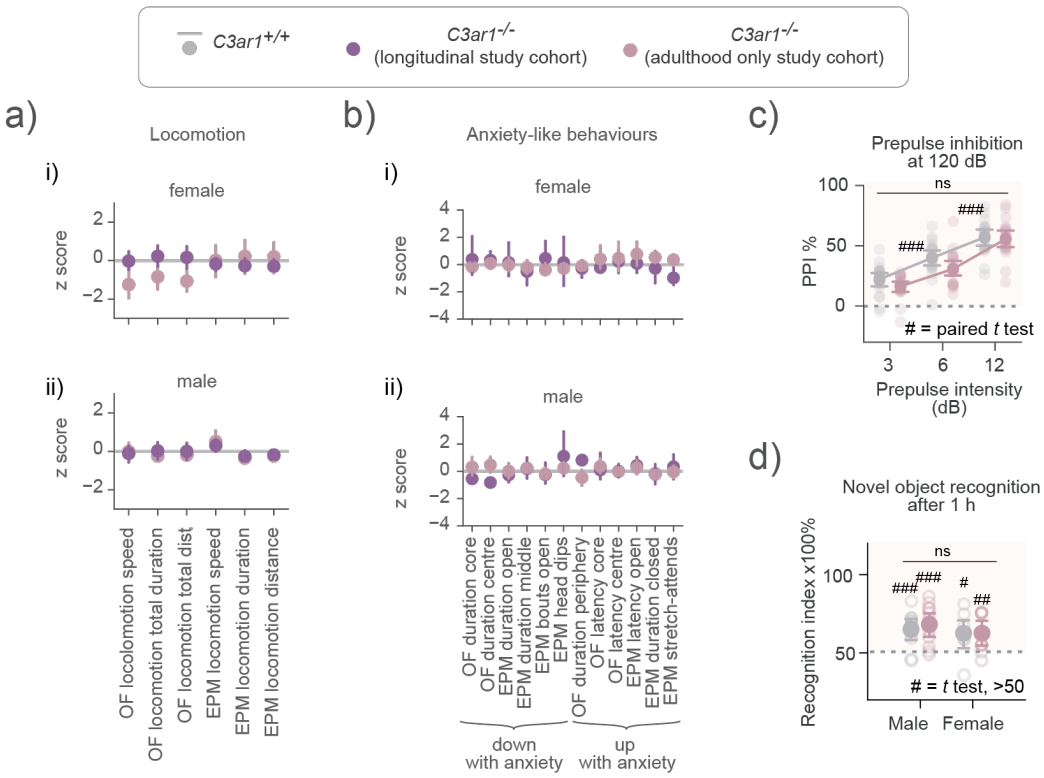

Figure 6 | *C3ar1* deficiency does not cause behavioural abnormalities. (a) Z-scored (normalised to *C3ar1*$^{+/+}$ control mean = 0) locomotion metrics for *C3ar1*$^{-/-}$ animals from EPM and OF tests, showing results from two independent study cohorts. Two-way ANOVA for longitudinal study (4 groups, males and females separated) or Student's *t* tests for the adulthood-only study cohort (2 groups, males and females combined due to smaller sample size) where parametric assumptions were met, otherwise the Kruskal Wallis test (with Dunn in the longitudinal study cohort); uncorrected for multiplicity, all ns. **(b)** Same as (a) but for anxiety-like metrics from EPM and OF tests; *p* values all ns. **(c)** Prepulse inhibition in the adulthood-only study cohort. PPI increased with increasing prepulse intensity in both, *C3ar1*$^{+/+}$ vs *C3ar1*$^{-/-}$ mice (paired *t* tests p value ### < 0.001). Dotted line at 0 indicates inhibition threshold. A score above 0 indicates inhibition (shaded area). Slope plot shows means and 95% confidence intervals. Individual mice are plotted three times at increasing prepulse intensity. Prepulse inhibition did not differ by genotype at any prepulse intensity (uncorrected Student's *t* tests at 3 dB, 6 dB and 12 dB, $t_{[37]}$ = 1.58, 1.99, 0.28, p = 0.12, 0.54, 0.17). **(d)** Novel object recognition (NOR) recall 1 hr after acquisition in the adulthood-only study cohort. Both groups showed novelty preference (one-sample *t* test, value > 50/chance, # = $p < 0.05$, ## = $p < 0.01$ ### = $p < 0.001$). There were no differences between groups (Student's *t* test $t_{[37]}$ = 0.42, p = 0.67). The dotted line marks the chance threshold. **(a-d)** Adulthood-only study cohort *C3ar1*$^{-/-}$ n = 20, *C3ar1*$^{+/+}$ n = 19 (males and females combined), longitudinal study cohort: *C3ar1*$^{-/-}$ n = 33 (17 male, 16 female), *C3ar1*$^{+/+}$ n = 33 (16 male, 17 female). Data are expressed as mean ± 95% CI.

1500 # Tables

1501 **Table 1 | Mean network connectivity metrics ± 95% CI in males and females**
1502 **of both genotypes**

Age	Adolescence				Adulthood			
C3ar1 status	+/+	-/-	+/+	-/-	+/+	-/-	+/+	-/-
Sex	F	F	M	M	F	F	M	M
Connectivity metric (AUC ± 95% CI)								
FC	25.5 ± 2	27.5 ± 3.1	25.9 ± 5	29.5 ± 4.5	27.6 ± 3.3	28.9 ± 2.9	29.9 ± 5.3	31.9 ± 4.7
GE	11.5 ± 0.8	12.7 ± 1.2	11.4 ± 1.5	13.2 ± 1.7	12.17 ± 1.2	12.9 ± 1.3	13.3 ± 2	14.5 ± 2.1
CC	13.5 ± 1.1	14.9 ± 1.9	13.9 ± 2.8	15.9 ± 2.6	14.8 ± 2	15.8 ± 1.9	16.3 ± 3.2	17.4 ± 2.6

1503

1504 **Table 2 | Mean anxiety-associated node connectivity in males and females of**
1505 **both genotypes.**

Age	Adolescence				Adulthood			
C3ar1 status	+/+	-/-	+/+	-/-	+/+	-/-	+/+	-/-
Sex	F	F	M	M	F	F	M	M
Brain area (mean node connectivity strength)								
L cingulate cx	0.39	0.41	0.39	0.44	0.45	0.49	0.48	0.54
R cingulate cx	0.38	0.41	0.38	0.43	0.45	0.49	0.48	0.53
L prefrontal cx	0.29	0.33	0.32	0.37	0.41	0.44	0.37	0.49
R prefrontal cx	0.28	0.28	0.33	0.37	0.41	0.45	0.39	0.47
L amygdala	0.14	0.17	0.15	0.2	0.2	0.2	0.24	0.28
R amygdala	0.11	0.16	0.15	0.18	0.19	0.2	0.25	0.25
L pallidum & accumbens	0.23	0.27	0.23	0.31	0.3	0.29	0.35	0.4
R pallidum & accumbens	0.24	0.26	0.24	0.3	0.31	0.31	0.35	0.39
L striatum	0.28	0.32	0.3	0.36	0.32	0.36	0.4	0.43
R striatum	0.26	0.31	0.32	0.35	0.33	0.36	0.42	0.41
L hypothalamus	0.28	0.29	0.27	0.34	0.32	0.32	0.34	0.38
R hypothalamus	0.25	0.27	0.26	0.32	0.31	0.32	0.33	0.37
L dorsal hippocampus	0.4	0.43	0.42	0.49	0.44	0.46	0.48	0.52
R dorsal hippocampus	0.41	0.43	0.42	0.49	0.44	0.47	0.5	0.52
L ventral hippocampus	0.18	0.18	0.17	0.26	0.21	0.23	0.2	0.27
R ventral hippocampus	0.18	0.23	0.19	0.25	0.22	0.25	0.25	0.26

L PAG	0.28	0.3	0.3	0.38	0.27	0.3	0.32	0.36
R PAG	0.28	0.31	0.3	0.39	0.27	0.29	0.32	0.37
L brain stem	0.11	0.11	0.12	0.18	0.1	0.14	0.16	0.16
R brain stem	0.11	0.09	0.12	0.18	0.11	0.13	0.17	0.18

Table 3 | Mean behavioural outcome measures ± 95% CI in males and females of both genotypes

Cohort	Cohort 1				Cohort 2			
Sex	F		M		F		M	
C3ar1 status	+/+	-/-	+/+	-/-	+/+	-/-	+/+	-/-
Locomotion-related								
OF locomotion speed (mm/s)	79.65±3.47	79.48±3.91	75.61±4.31	74.72±4.08	94.21±6.64	84.33±7.26	84.93±7.55	84.93±5.68
OF locomotion duration (s)	213.38±22.53	223.73±26.85	216.60±21.94	217.97±20.82	315.66±50.93	264.33±49.90	297.85±39.56	283.61±17.86
OF locomotion distance (cm)	1777.89±210.25	1847.71±271.41	1746.45±257.47	1747.52±225.53	2984.99±589.73	2231.45±473.78	2562.36±515.37	2412.03±268.13
EPM speed (mm/s)	67.07±3.43	65.89±2.40	67.71±3.74	69.90±2.60	75.27±5.08	75.38±6.40	73.61±4.21	76.63±3.76
EPM locomotion duration (s)	69.25±15.36	61.22±11.89	73.29±13.14	67.01±7.48	78.93±13.23	82.53±18.41	71.11±17.69	62.51±8.88
EPM locomotion distance (cm)	473.32±124.87	401.52±88.01	502.39±109.22	465.16±54.60	591.26±122.20	620.88±155.69	518.89±140.06	472.57±68.28
Anxiety-related								
OF duration core (s)	25.92±12.12	18.74±4.60	19.81±5.35	22.99±7.73	25.06±10.65	29.96±24.36	32.19±18.93	16.71±3.87
OF duration centre (s)	106.94±18.40	102.01±16.36	97.18±13.68	109.40±17.99	105.42±40.78	120.94±39.65	133.80±31.20	95.62±13.10
OF duration periphery (s)	493.13±18.41	498.07±16.36	502.90±13.68	490.66±17.98	493.16±42.58	478.89±39.60	466.11±31.25	504.15±13.10
EPM duration open (s)	29.52±11.52	28.92±12.57	28.06±12.03	28.19±14.72	18.87±8.77	20.45±16.56	15.13±7.96	12.15±7.29
OF latency core (s)	30.66±17.23	44.47±34.34	29.89±16.18	40.95±19.45	34.19±36.91	24.15±20.50	25.86±25.45	29.44±52.19
OF latency centre (s)	10.02±3.52	13.26±8.07	12.35±7.40	11.97±4.95	5.79±6.00	7.45±7.79	5.22±5.01	5.28±4.26
EPM duration middle (s)	109.53±17.89	102.17±19.15	112.33±24.24	122.79±17.27	85.38±21.11	72.59±29.02	71.13±14.54	74.93±17.85
EPM duration closed (s)	176.11±22.18	198.69±19.25	188.78±24.17	178.29±17.22	214.24±21.04	207.31±38.82	227.88±14.86	224.17±17.79
EPM bouts open (#)	4.65±1.92	3.19±1.66	3.44±1.33	2.94±1.18	2.62±1.48	3.43±2.77	2.30±1.12	1.91±1.49
EPM head dips (#)	21.53±6.20	18.12±5.17	19.62±6.29	22.31±5.36	16.75±4.55	17.57±13.16	11.90±3.14	16.73±8.52

EPM stretch-attend postures (#)	19.00±4.15	21.81±2.98	23.62±3.14	23.38±2.87	16.62±6.16	9.43±6.04	13.50±2.68	14.73±4.10
EPM latency open (s)	65.31±27.63	106.76±53.38	92.95±48.81	117.27±51.75	75.66±81.38	83.26±103.55	95.40±71.29	137.52±70.66
Other								
PPI 3 dB (%)					21.11±13.2	15.31±6.40	22.87±7.41	17.14±7.70
PPI 6 dB (%)					40.63±10.16	26.36±8.74	39.49±11.24	34.37±10.65
PPI 12 dB (%)					56.81±13.18	49.81±13.28	57.07±9.51	60.40±8.38
Acoustic startle response at 120 dB (A.U.)					876.35±432.36	1068.32±284.31	1472.99±360.84	1908.79±655.66
NOR recognition index (%)					62.49±11.20	62.60±9.77	65.02±7.66	68.16±8.87
NOR total exploration training (s)					39.45±15.62	38.58±10.66	38.50±12.16	41.12±11.07
NOR total exploration test (s)					31.68±10.07	32.41±6.83	30.81±9.17	33.58±5.39